Wind-driven hydrodynamic and depositional patterns in shallow lakes

An exploratory modelling approach based on an archetypal case of Lake Hulun

Xue, Xinyu; Storms, Joep; Zăinescu, Florin; Schuster, Mathieu; Wang, Li; May, Jan Hendrik; Ng, Zhi Lin; van der Vegt, Helena; Jiang, Zaixing; More Authors

DOI
10.1111/sed.13265

Publication date
2025

Document Version
Final published version

Published in
Sedimentology

Citation (APA)
Xue, X., Storms, J., Zăinescu, F., Schuster, M., Wang, L., May, J. H., Ng, Z. L., van der Vegt, H., Jiang, Z., & More Authors (2025). Wind-driven hydrodynamic and depositional patterns in shallow lakes: An exploratory modelling approach based on an archetypal case of Lake Hulun. *Sedimentology*, *72*(4), 1040-1064. https://doi.org/10.1111/sed.13265

SEDIMENTOLOGY the journal of the International Association of Sedimentologists IAS

Sedimentology (2025) doi: 10.1111/sed.13265

Wind-driven hydrodynamic and depositional patterns in shallow lakes: An exploratory modelling approach based on an archetypal case of Lake Hulun

XINYU XUE*,†,‡, JOEP STORMS†, FLORIN ZĂINESCU§,¶, MATHIEU SCHUSTER**, LI WANG‡,**, JAN-HENDRIK MAY††, ZHI LIN NG*, HELENA VAN DER VEGT‡‡, ALEXIS NUTZ§, GUILHERME BOZETTI**, MING SU* and ZAIXING JIANG‡

**School of Marine Science, Sun Yat-sen University, Zhuhai 519083, China*
(E-mail: xuexy9@mail.sysu.edu.cn)
†Department of Geoscience and Engineering, Delft University of Technology, Delft 2628, The Netherlands
(E-mail: j.e.a.storms@tudelft.nl)
‡School of Energy Resources, China University of Geosciences, Beijing 100083, China
(E-mail: Jiangzx@cugb.edu.cn)
§Aix Marseille University, CNRS, IRD, INRAE, Coll France, CEREGE, Europole Méditerranée de l'Arbois BP 80 13545 Aix-en-Provence cedex 04, France
¶SCMF, Faculty of Geography, University of Bucharest, 1 N. Balcescu Blv., Bucharest 010041, Romania
***Université de Strasbourg, CNRS, ENGEES, Institut Terre et Environnement de Strasbourg, UMR 7063, 5 rue Descartes, Strasbourg F-67084, France*
††School of Geography, Earth and Atmospheric Sciences, University of Melbourne, 253 Elgin St., Carlton 3053,Vic., Australia
‡‡Deltares, Delft 2600MH, The Netherlands

ABSTRACT

Lake Hulun, the fifth-largest lake in China, is a shallow lake (water depth <10 m) with typical wave-dominated landforms developed around the shoreline, with a semi-enclosed bay located in its southern corner. This novel study aims to understand wind-driven hydrodynamics and its related depositional patterns in the data-sparse Lake Hulun. To achieve this, a series of numerical simulations were conducted with a hydrodynamic and sediment transport model. The simulated hydrodynamic patterns are greatly influenced by wind direction shifts but are subject to little impact from wind speed changes which act mainly to accelerate flow. By varying the location and depth of the deepest part of the lake, this study reveals that the location of the depth centre has little impact on the overall hydrodynamic pattern of wind-driven waterbodies. When the wind direction is perpendicular to the long-axis shore, currents around the short-axis shore flow in a direction that follows the wind direction. This study considers the wind-induced longshore currents that are oblique to the long-axis shore as the main driving force in transporting sediments along the shore and erosion of the shoreline. The formation of semi-closed bays in both Lake Hulun, together with its nearby sister lake – Lake Buir – are attributed to the north-west prevailing wind direction. Further exploratory simulations confirmed that prevailing winds tend to induce parallel distributed submerged sediment accumulations in the nearshore zone, challenging the notion of sediment accumulation solely in deep water zones. This study provides valuable insights into the hydro-sedimentary dynamics in wind-driven waterbodies, offering a

process-based perspective and contributing to current understanding of the palaeogeography of ancient lake systems.

Keywords Delft3D, hydrodynamics, Lake Hulun, littoral landforms, wind-driven waterbody.

INTRODUCTION

Understanding sedimentation patterns in lakes is crucial for reconstructing past climate variability, landscape evolution, ecological shifts and human impacts in lake and watershed ecosystems over centennial to millennial timescales (Cohen, 2003). While sedimentation in lakes has been regarded as a simple process when compared to the ocean, recent research indicates that the littoral sedimentation in lakes is quite similar to that of ocean coasts, except for tide influences (Gracia *et al.*, 2021). Lakes influenced by prevailing winds often exhibit an asymmetrical deposition pattern with river-dominated or gravity-dominated shorelines upwind and wave-dominated shorelines downwind. This pattern thereby reflects the prevailing wind direction and has been observed in numerous examples from both the Holocene and ancient lakes (Jiang *et al.*, 2011, 2018; Schuster *et al.*, 2014; Schuster & Nutz, 2018; Wang *et al.*, 2018; Nutz *et al.*, 2020; Xue *et al.*, 2021; Wang *et al.*, 2024). Recently, Nutz *et al.* (2018) proposed a novel classification of lakes called 'wind-driven waterbodies' (WWB) to describe lakes with coastal sedimentary features produced by wind-driven waves and currents. The specific landforms produced by such wave-related processes are spits, barriers and berms on the lake shore (Schuster *et al.*, 2014; Schuster & Nutz, 2018; Nutz *et al.*, 2020). Compared to a lake with an asymmetrical deposition pattern, the 'WWB' lake type defined by Nutz *et al.* (2015, 2018) is characterized by wave-related landforms along more than 80% of the shoreline. These WWBs generally feature a relatively shallow water depth relative to their size. A WWB-Index (I_{WWB}) has been introduced as the ratio of fetch (km) to water depth (m), which allows the distinguishment of wave-driven waterbodies (I_{WWB} superior to three) from other waterbodies (Nutz *et al.*, 2018).

Wind-driven bottom currents, analogous to marine contourite systems, have been documented in several large lakes. For instance, seismic evidence from Lake Baikal revealed small-scale lacustrine drifts generated by persistent bottom currents (Ceramicola *et al.*, 2001), while Late Pleistocene to Holocene contourite deposits in Lake Prespa demonstrate the long-term significance of wind-driven bottom circulation in controlling sediment distribution patterns (Wagner *et al.*, 2012). These currents play a crucial role in sediment transport on the lake floor, while the flow circulation controls the evolution of landforms at the lake coast (Nutz *et al.*, 2015, 2018).

The quantitative analysis of wave-related sedimentation in lakes is complex because sediments tend to be resuspended within shallow marginal areas and are transported progressively to deeper waters (e.g. Luettich Jr. *et al.*, 1990; Bengtsson & Hellström, 1992; Morales-Marin *et al.*, 2018). In shallow lakes where the I_{WWB} can be much larger than the threshold of WWB, wind waves are able to induce turbulence and potentially resuspend sediments from the lake floor throughout the entire lake area (Jin & Ji, 2004; Kazancı *et al.*, 2010). The sediment resuspension process occurs for conditions that correspond to a specific water depth and wind speed (Luettich Jr. *et al.*, 1990; French *et al.*, 2000). Morales-Marin *et al.* (2018) demonstrated that wave-generated bottom stresses are the main mechanism for sediment focusing in shallow near-shore waters (less than 3 m depth), whereas wind-driven currents are the dominant contributor to bottom stress in deeper waters (Nutz *et al.*, 2015). Despite these advances, there remains a significant knowledge gap regarding the flow circulation under more complex wind conditions, where its understanding will have implications for lacustrine hydrology, ecology and sedimentology.

Given the complexities of lake hydrodynamics, which are controlled by multiple factors, such as river influx, winds, wave generation, salinity, bathymetry, topography and thermal force, numerical modelling has emerged as a useful approach to understand the circulation, mixing and stratification processes, allowing for delineating sediment transport, deposition patterns and associated environmental impacts

(Morales-Marín *et al.*, 2017). Several studies have successfully applied numerical modelling to investigate the hydro-sedimentary dynamics in great lakes with greater depth, such as Lake Strynevatnet (Norway; Storms *et al.*, 2020) and Lake Turkana (Kenya; Zăinescu *et al.*, 2023). Lake Michigan (USA) has also been extensively studied in terms of sediment drift, transport and settlement processes, influenced by various factors, including wind, wave and heat flux transfer (Mao & Xia, 2020; Khazaei *et al.*, 2021). However, relatively little attention has been given to simulation studies in WWBs (Gracia *et al.*, 2024). Previous simulation studies have typically used dynamic wind sets over long-term scales, ranging from seasonal to annual (e.g. Mao & Xia, 2020), while the systematic analysis of hydro-sedimentation response towards discrete wind parameters (direction, speed) remains insufficiently quantified.

Lake Hulun is a lake in China exhibiting typical coastal landforms along the shoreline, including a large semi-enclosed bay. It is also characterized by shallow depth relative to its area (Fan *et al.*, 2021). While some large-scale sandy beach ridges and spits are well-developed on the downwind-side shore of the lake, there are also many wave-related landforms on the upwind-side shore (Wang *et al.*, 2024). Therefore, Lake Hulun contains all of the elements required to be identified as a WWB. Several studies on Lake Hulun focused on selected aspects related to the impact of wind, such as the distribution of organic carbon and nutrient elements (Chen *et al.*, 2021; Li *et al.*, 2021). Nonetheless, there remain questions about the underlying mechanisms behind the development of wave-related landforms related to the wind-driven hydrodynamics and its related sedimentation around the shoreline of Lake Hulun.

This paper examines a diverse set of process-based simulations of Lake Hulun to investigate hydrodynamic and sedimentation characteristics under specific wind fields with varying directions and velocities, over a temporal scale ranging from days to months. Then the impact of uncertainties in bathymetry and shoreline configuration on hydrodynamics and sedimentation is explored. This study emphasizes the development of an exploratory modelling approach with sparse data constraints, where insight gained from it will provide a quantitative foundation for differentiating wave-dominated facies from other lacustrine deposits, thereby enhancing our ability to reconstruct ancient atmospheric circulation patterns from the geological record. Through a systematic analysis of these numerical simulations, three main research questions are addressed and discussed: (i) the quantitative relationships between wind-field parameters and the resultant hydrodynamic–sedimentary responses in WWBs; (ii) the mechanistic controls on distinctive littoral landform development, specifically focusing on the formative processes of a semi-enclosed bay in Lake Hulun; (iii) the implications of sediment erosion and accumulation patterns in Lake Hulun for interpreting depositional architectures in ancient wind-driven lake systems.

STUDY AREA

Geographical settings

Lake Hulun, located in the north-east of China close to the borders of Russia and Mongolia (Fig. 1A), is the fifth-largest lake in China with a unique irregular oblique rectangle shape. The lake has a mean water depth of 5.75 m, water storage capacity of 13.85×10^9 m^3 and water area of 2134 km^2 at the water level of 544 m, as measured in 2019 (Zheng *et al.*, 2016; Chen *et al.*, 2021). The lake has a maximum length of 93 km and width of 41 km, elongated in a north-east/south-west direction. Fluvial and alluvial plains are found along the south-eastern shorelines. Meanwhile, low mountains and hills built by Mesozoic volcanic rocks form a fault-scarp lake shoreline on the north-western side (Cai *et al.*, 2016). Over 60 rivers and streams feed Lake Hulun, with the Krulen and Urshen rivers serving as the primary sediment source (Cai *et al.*, 2016). The Krulen River originates in the upper parts of the Khentii mountain in eastern Mongolia and flows eastwards to Lake Hulun in China (Gao *et al.*, 2017). As a part of the hydrological system of the Khalkha River, the Urshen River receives outflow water from Lake Buir before flowing north towards Lake Hulun (Fan *et al.*, 2021). The Xinkai River, located in the north-eastern part of the lake, has been cut off since 1998, turning Lake Hulun into an enclosed lake without outflows (Cai *et al.*, 2016). Lake Hulun is an endorheic lake situated in a mid-high latitude temperate semi-arid zone, where the regional climate is controlled by the Westerlies and East Asian monsoon systems (Xiao *et al.*, 2009). Mean annual temperature is

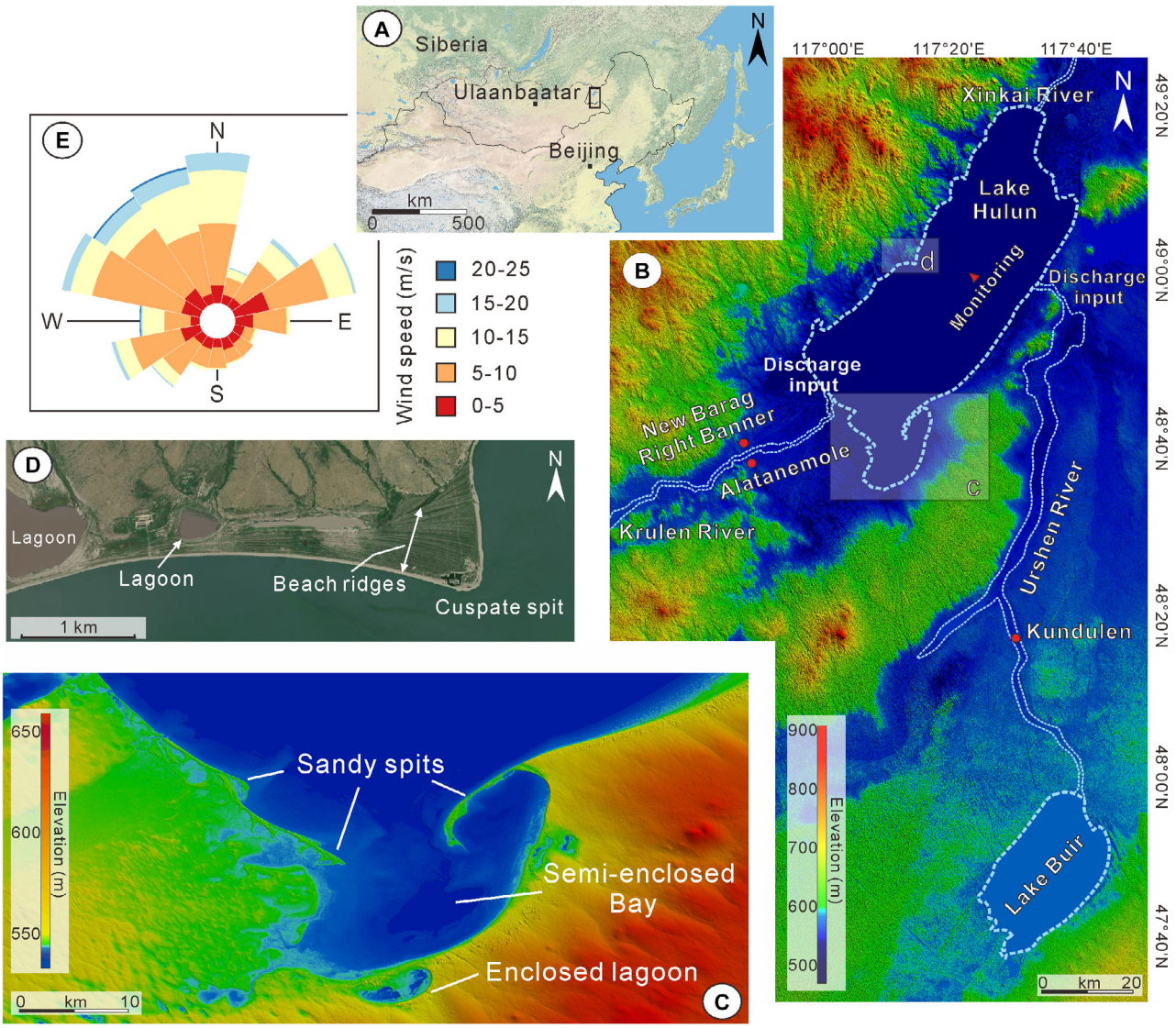

Fig. 1. (A) Geographic location of Lake Hulun. Black box indicates the location of panel (B). (B) Digital elevation model (DEM; GLO-30 provided by Open Topography through the public AWS S3 bucket) of Lake Hulun and its main drainage network. The red dots represent the locations of meteorological and hydraulic stations. (C) A zoomed-in DEM of the appendix lake of Lake Hulun. (D) A satellite image captured from EsriChina (Environmental Systems Research Institute) of the cuspate foreland in 2010. (E) Windrose diagram of the non-frozen days from 2011 to 2020, recorded by the New Barag Right Banner station.

0.3°C, with significant seasonal amplitude ranging from −21°C in January to 20°C in July. The frozen period of Lake Hulun is from October to March, during which the ice cover progressively develops from the margins to the lake centre until the lake is completely ice-bound (Cai *et al.*, 2016; Ao *et al.*, 2020). The area experiences an annual average precipitation of 290 mm, with more than 80% occurring during June to September (Cai *et al.*, 2016). Evaporative water loss represents the predominant hydrological egress pathway from Lake Hulun, with river discharge, groundwater influx and direct precipitation collectively replenishing the system at a proportional ratio of approximately 5 : 3 : 2, respectively (Sun *et al.*, 2018).

Littoral landforms

A comprehensive geomorphological and sedimentological analysis of the littoral landforms surrounding Lake Hulun has been systematically

documented through integrated satellite imagery interpretation and field investigations (Wang *et al.*, 2024). These observations provide critical ground-truth validation for the modelling work in this paper.

A series of spits occurs around the shoreline of Lake Hulun, of which the most prominent ones (4–7 km in length) can be found near the semi-enclosed bay situated in the southern corner of the lake (Fig. 1C). These spits show characteristic recurved terminations with associated salt marsh development in their lee. A cuspate spit is located along the central section of the north-western shoreline. This cuspate spit comprises a sequence of beach ridges spanning 1 km in width (Fig. 1D). The morphology exhibits asymmetrical development with a short erosional side and an elongated depositional side, preserving evidence of progressive shoreline progradation (Wang *et al.*, 2024). Several wave-dominated deltas fed by braided rivers originating from the north-western valleys also developed on the north-western shore (Fig. S1A and S1B). The south-eastern shore is characterized by a wide-open floodplain (Fig. 1B). A laterally extensive beach develops along the south-eastern coast of the lake, oriented perpendicular to the incoming waves (Wang *et al.*, 2024). A barrier island also appears in the estuary area of Xinkai River (Fig. S1C). The littoral landforms described above demonstrate the dynamic nature of lake coasts in response to wind-induced waves. In addition, aeolian deposits are predominantly developed along the eastern shoreline in the form of a kilometre-wide coastal dunes system (Wang *et al.*, 2024). The extension direction of these dunes indicates a dominant north-westerly wind regime (Fig. S1E).

PRINCIPLES AND METHODS

Delft3D model description

This study utilizes the Delft3D (v4.04.01), an open-source software package developed by Deltares (Delft, The Netherlands), to simulate hydrodynamics and non-cohesive sediment transport in Lake Hulun (Lesser *et al.*, 2004). The hydrodynamic module (Delft3D-FLOW) solves the three-dimensional incompressible Reynolds-averaged Navier–Stokes (RANS) equations and is coupled with the third generation Simulating Waves Nearshore (SWAN) wave model which incorporates wave processes and wave-induced bed shear stresses responsible for sediment resuspension (Deltares, 2021). The SWAN model, which solves the discrete spectral balance of action density, was used to simulate wave generation and propagation (refraction and shoaling) in Lake Hulun. The effects of wind growth are added to the simulation and are combined with the effects of wave dissipation due to whitecapping, bottom friction and wave breaking. The computed wave field is coupled to the FLOW module through a 'communication file', ensuring a dynamic two-way wave-current interaction (Deltares, 2021). The non-cohesive sediment transport is simulated following the formulation of Van Rijn (2007a), and is fully coupled with the hydrodynamics in the FLOW module.

Data acquisition

Bathymetry

The yearly water level fluctuation of Lake Hulun from 1992 to 2022, derived from satellite altimetry data, is recorded in the Hydroweb database (https://hydroweb.theia-land.fr/), which was created by LEGOS (Laboratoire d'études en Géophysique et océanographie spatiales). The elevation of the water level ranges from 539.5 to 545.5 m (Fig. 2A), documenting a minimum of 6 m variation in water depth.

The Copernicus Digital Elevation Model (GLO-30) was applied to draw the contours of the water–land region with incomplete coverage of the lake and catchment at the water level of 543 m (Fig. 1B and 1C). A local depression (depth centre) exists towards the deeper area of Lake Hulun, where its depth and location are uncertain due to sparse data. The location of the depth centre was set initially according to the study by Fan *et al.* (2021) who obtained the depth contours using an autonomous surface vehicle (ASV), indicating a maximum water depth of approximately 8 m. Finally, a complete bathymetric map was weaved for the simulation work in this study (Fig. 3A).

River discharge

The Krulen and Urshen rivers are the main contributors of the discharge input to Lake Hulun. The inflows from these rivers are limited due to low precipitation. According to the records from hydrological stations of Alatanemole and Kunduleng (see locations in Fig. 1B), which represent the discharge into Lake Hulun from the

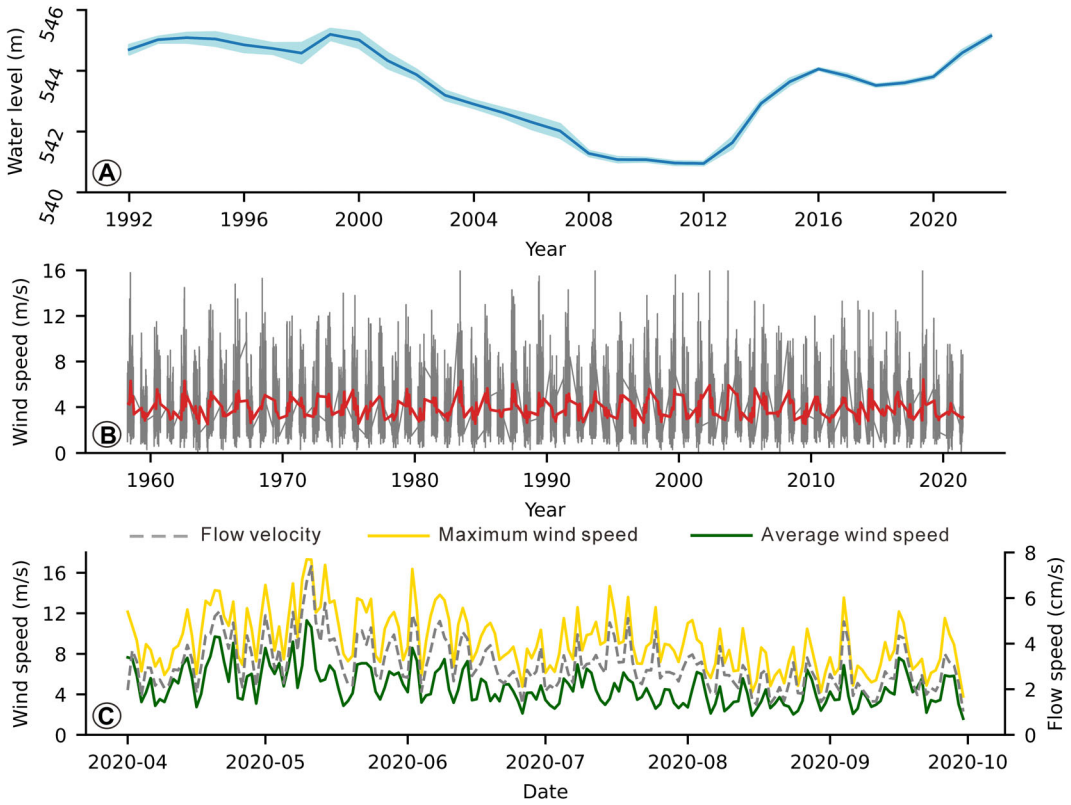

Fig. 2. (A) Water level from 1992 to 2022 with 95% confidence interval. (B) Daily-averaged wind speed (grey line) and monthly-averaged wind speed (red line) for non-frozen days from 1958 to 2021. (C) Wind speed from April to September 2020, and the simulated bottom flow speed in the depth centre (Point B, see location in Fig. 3) under daily averaged wind velocity (Scenario 2a). All wind data are recorded at New Barag Right Banner Station.

Krulen and Urshen rivers, the mean annual discharge, respectively from the two largest rivers, was 198 m^3/s for Urshen River and 172 m^3/s for Krulen River. An artificial dam is located upstream of Xinkai River to adjust the water level in a stable range (Fig. S1D).

Physical conditions

The salinity ranges between 1466 and 2395 mg/L from 1999 to 2011 (Gao *et al.*, 2017), which is close to the freshwater standard (1000 mg/L). Lake Hulun is controlled by monsoons from the Mongolian Plateau and the North Pacific Ocean (Li *et al.*, 2021). The prevailing wind direction around Lake Hulun during the non-frozen season is north-west with average velocities of around 3 to 6 m/s (Figs 1E and 2B). Grain-size analysis from Sun *et al.* (2018) revealed that the sediment bed of Lake Hulun consists mainly of fine-grained silts to very fine-grained sands.

Model setup

Table 1 presents a list of key modelling parameters defined in the simulation scenarios. The Lake Hulun area is represented by a structured grid with equal-sized cells of 450 × 450 m (Fig. 3A). A total of 20 σ-layers were used to define the vertical water column, of which the thickness proportion is 2% for each of the surface and bottom, and 6% for each of the middle 12 layers. Thus, the maximum σ-layer thickness is 0.48 m. The model has a timestep of 30 s, and is coupled with the wave field in every 2 h. To ensure the orthogonality between the lake shoreline and the model grids, a counter-clockwise rotation of 37° is applied to the grid model of Lake Hulun. All corresponding wind direction inputs are also compensated by a similar rotation of 37° in alignment with the grid model.

Two input boundaries are set at the river mouth of the Krulen and Urshen rivers, which are forced

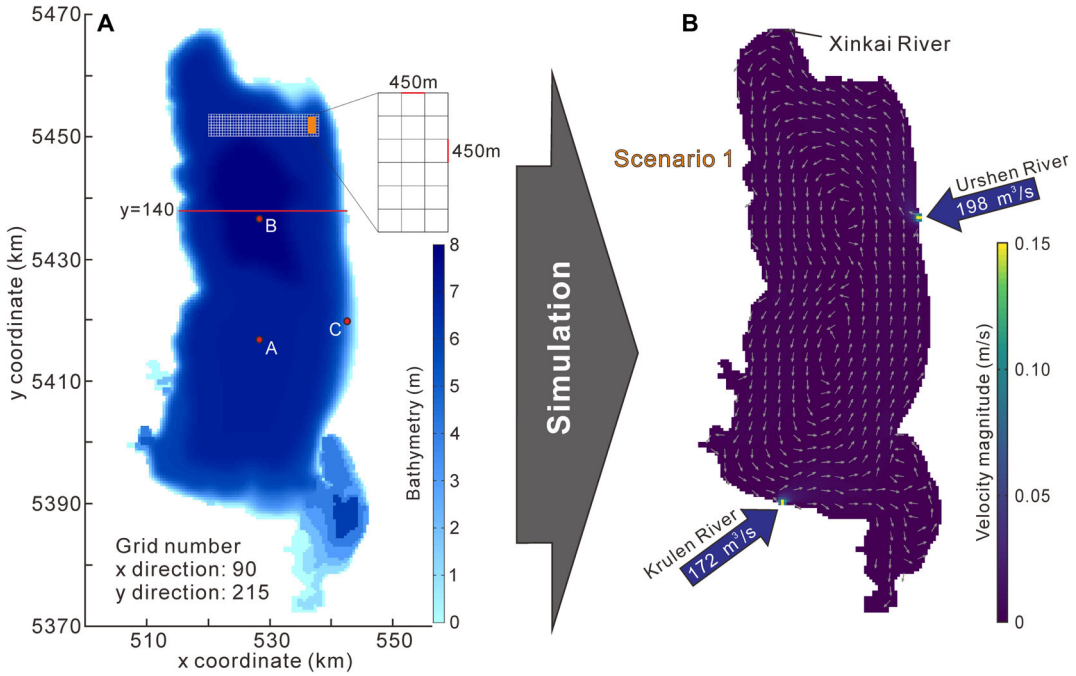

Fig. 3. (A) Complete bathymetry of Lake Hulun and the grid information. Red dots ('A', 'B' and 'C') are simulation observation points. (B) Boundary conditions for all scenarios and the simulation result of Scenario 1. The white arrows represent flow vectors, which show consistent patterns through all vertical layers.

by a total discharge of 198 and 172 m^3/s, respectively (Fig. 3B). Both input boundaries have a uniform suspended sediment concentration of 1 kg/m^3 over the simulation. A water-level boundary was imposed at the outflow point of Xinkai River so that water does not overflow out of the lake under the continuous inflows of the Krulen and Urshen rivers. The yearly mean wind velocity in the study area is 4 m/s (1960–2021), with daily maximum velocities frequently reaching 12 m/s (Fig. 2B). A uniform wind speed of 12 m/s, representing a commonly observed extreme wind condition around Lake Hulun, is implemented in the baseline scenarios to ensure sufficient bed shear stress for sediment mobilization while maintaining realistic environmental parameters.

Three observation points were set up in the model (Fig. 3A). Given that Lake Hulun approximates freshwater conditions, salinity effects were not included in the model. The temperature differences both inside the shallow waterbody and between the lake and the inflowing waters are negligible, thus temperature-induced density variations were also excluded from the model. The initial bed thickness of the lake substrate is 1 m, composed of non-cohesive sediments with the D50 as 100 μm, which correspond to very fine-grained sands. The physical properties of the input sediment are parameterized identically to the bed substrate. The lake floor roughness is implemented by the Manning formulation using a uniform value of 0.03 s $m^{(-1/3)}$, which is considered as the representative value for a natural system with sands and vegetation (Arcement & Schneider, 1989). The bottom friction is defined in the SWAN model by the JONSWAP model (Hasselmann *et al.*, 1973) with a bottom friction coefficient of 0.067 m^2/s^3. A spin-up time of 720 min is set for each simulation before morphological updating begins. During this time interval, there are no morphological changes. The wave processes are implemented by using the third-generation Simulating Waves Nearshore (SWAN) wave model (Booij *et al.*, 1999) coupled to the Delft3D-Flow module.

Scenario design

A series of scenarios were designed and grouped into four sets, each focusing on a different variable, including wind condition, bathymetry, shoreline configuration and hydrodynamic time, to test the sensitivity of each variable on the hydro-sedimentary dynamic response. Each

Table 1. Key parameters for simulation.

Parameter	Value
Timestep	30 s
Grid cell dimension in M and N	450 × 450 m
σ layers	20
Sediment grain size (D50)	100 μm
Initial bed thickness	1 m
Hydrodynamic time	Four days
Morphological scaling factor	1
Spin-up time	720 min
Manning coefficient	0.03 s $m^{-1/3}$
Turbulence model	K-ε
Horizontal eddy viscosity	2 m^2/s
Horizontal eddy diffusivity	0.7 m^2/s
Sediment transport formula	TRANSPOR2004 (Van Rijn, 2007a)
Specific bed density of sediments	2650 kg/m^3
Dry density of sediments	1600 kg/m^3
Wave-related bed-load transport factor	0.2
Wave breaker index	0.73

scenario is described in detail below and summarized in Table 2.

Scenarios with variable wind conditions

To assess the impact of wind on the flow circulation of Lake Hulun and its effects on sedimentation pattern, this scenario group uses multiple wind conditions, starting from Scenario 1 (S1) without wind influence. Scenario 2 (S2) included wind influence with a wind direction of 315°, perpendicular to the long-axis shore. Three subsequent rotations of a 22.5° interval in both the clockwise and counter-clockwise directions were applied, making up a total of seven distinct wind direction scenarios (from south-west to north-east: 247.5°, 270°, 292.5°, 315°, 337.5°, 0°/360° and 22.5°). The wind direction is kept at 315°, with variations in wind speed from 6 to 18 m/s set for Scenario 3 (S3).

Scenarios with variable bathymetry

To assess the sensitivity to bathymetric uncertainty and to compare the circulation patterns produced by different bathymetric maps, three further experimental scenarios were created (S4a–S4c), following up on the earlier scenario groups with a constant bathymetric condition. Initially, a new bathymetric map with two depth centres according to Li *et al.* (2013) was inserted into Scenario 4a. Then, Scenario 4b was implemented with a deepened depth centre, which has a maximum water depth of 15 m. The final Scenario 4c exhibited an overall increase in water depth throughout the entire lake.

Scenarios with simplified shoreline shape

To assess the impact of irregular shoreline morphology, an idealized lake model with rectangular shoreline and bathymetric gradients are created for Scenario 5. The water depth and fetch distance are based on the Lake Hulun model. The wind direction is coming from the east (270°) and perpendicular to the long-axis shoreline in Scenario 5a. Due to the irregularity of lake shorelines in the real world and the hourly changes wind direction, it is necessary to consider the circulation pattern for non-idealized wind scenarios. Therefore, oblique wind directions (315° and 337.5°) are also inserted into Scenarios 5b and 5c.

Scenarios with half-year hydrodynamic time

To investigate the cumulative sedimentation and erosion generated by wind-driven flow circulation on a long-term scale, two scenarios with a half-year simulation period are designed. Firstly, the daily maximum wind velocities from April to September 2020 are implemented in Scenario 6a to examine the effects of shifting wind conditions on the hydrodynamics and sedimentation of Lake Hulun. Additionally, a constant wind field is implemented in Scenario 6b to reflect sedimentation processes under prevailing wind influence.

RESULTS

Wind variations

Scenario without wind input (Scenario 1)

Without winds, a counter-clockwise flow circulation develops in the lake (Fig. 3B), which is consistent for each vertical water layer. Only a small region near the river-mouth area of both the Krulen and Urshen rivers exhibits slightly higher velocities, whereas other parts of the water body have very low velocities (<0.05 m/s).

Table 2. Settings for each scenario group.

Scenario		Bathymetry	Wind direction	Wind speed
S1		One depth centre in the north (according to Fan *et al.*, 2021)	/	/
S2	a	One depth centre in the north (according to Fan *et al.*, 2021)	22.5°	12 m/s
	b		360°/0°	
	c		337.5°	
	d		315°	
	e		292.5°	
	f		270°	
	g		247.5°	
S3	a	One depth centre in the north (according to Fan *et al.*, 2021)	315°	6 m/s
	b			9 m/s
	c			15 m/s
	d			18 m/s
S4	a	Two depth centres (according to Li *et al.*, 2013)	315°	12 m/s
	b	Deepened depth centre		
	c	Overall depth increase		
S5	a	Simplified bathymetry	270°	12 m/s
	b		315°	
	c		337.5°	
S6	a	One depth centre in the north (according to Fan *et al.*, 2021)	Daily maximum wind speed for six months	
	b		Wind same as Scenario 2d for six months	

This flow pattern results in an overall very low suspended sediment concentration (SSC) across the lake, with the exception of the immediate vicinity of the Krulen and Urshen rivers (Fig. 4A).

Scenarios with variable wind directions (Scenario 2, a–g)

Imposed wind fields have a direct impact on the directions and velocities of simulated flow velocities in Lake Hulun and as such on the simulated suspended sediment concentrations in the water column. The simulated counter-clockwise rotating flow observed for Scenario 1 is overprinted by a strong surface and bottom flow for Scenario 2 (Fig. 5). Surface flow direction in the lake centre aligns with the wind direction in the upper 1 to 2 m of the water column. There is a clear bottom return flow in the opposite direction of the surface flow of up to 6 m thick, depending on the local lake depth. A reduced-flow layer separates the opposing surface and bottom flow (Fig. 6B). Simulated surface and bottom currents scale in their velocities with the imposed wind velocities, and are typically lower than 0.1 m/s for wind velocities below 12 m/s. However, they may reach 0.25 m/s for wind velocities of 18 m/s.

Overall, near-shore and shore parallel currents are significantly faster (0.25 m/s or higher) than currents in the lake centre, away from the lake shores. Surface flow velocities along the upwind shore are higher than the downwind shore when the wind direction is nearly perpendicular to the downwind shore (Fig. 5B to D). Complex flow patterns also arise in the semi-enclosed bay in the southern part of Lake Hulun (Fig. 5A to C), for conditions when the wind directions

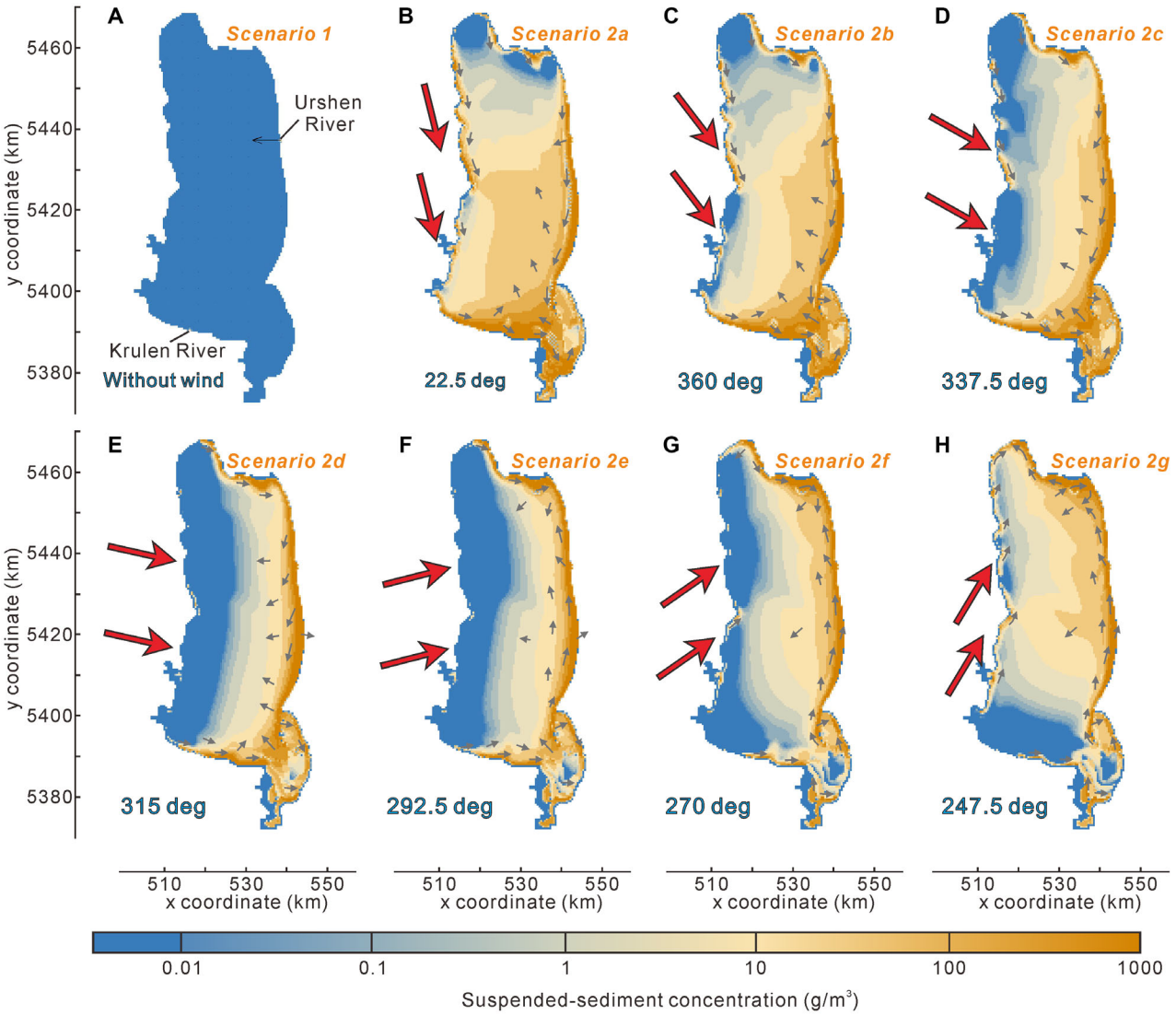

Fig. 4. Spatial distribution of suspended-sediment concentration at the bottom layer (layer 20) in (A) Scenario 1 and (B) to (H) Scenarios 2a to 2g. Grey arrows indicate the residual sediment transport direction.

range from 22.5° to 315° (S2a–S2d). Here, the flow velocity can also reach up to 0.25 m/s, especially when the wind direction is oblique to the long-axis shore (S2c).

As the wind direction changes, the distribution of SSC at the near-bed layers (represented by layer 20 in Fig. 4) shift. Overall, the near-bed SSC shows higher values on the downwind shore (Fig. 4). When the wind direction is oblique to the downwind shore, the upwind shore also exhibits higher SSC values (up to nearly 15 g/m^3, Fig. 4B, 4C, 4D, 4G and 4H) than that shown in Scenarios 2d and 2e (Fig. 4E and 4F).

The depth centre, which is located in the northern part of the lake, reduces the velocity of surface currents but increases the velocity of bottom currents, especially when the wind direction is nearly parallel to the long-axis shore. Contrary to the discernible influence of the depth centre on hydrodynamics, the SSC remains unaffected by the presence of a depth centre (Fig. 4).

Scenarios with variable wind velocities (Scenario 3, a–d)

To better understand the consistency of flow patterns for varying wind velocities, the relationship between wind force and flow behaviour was also tested. For a wind direction of 315°, which is perpendicular to the downwind shore,

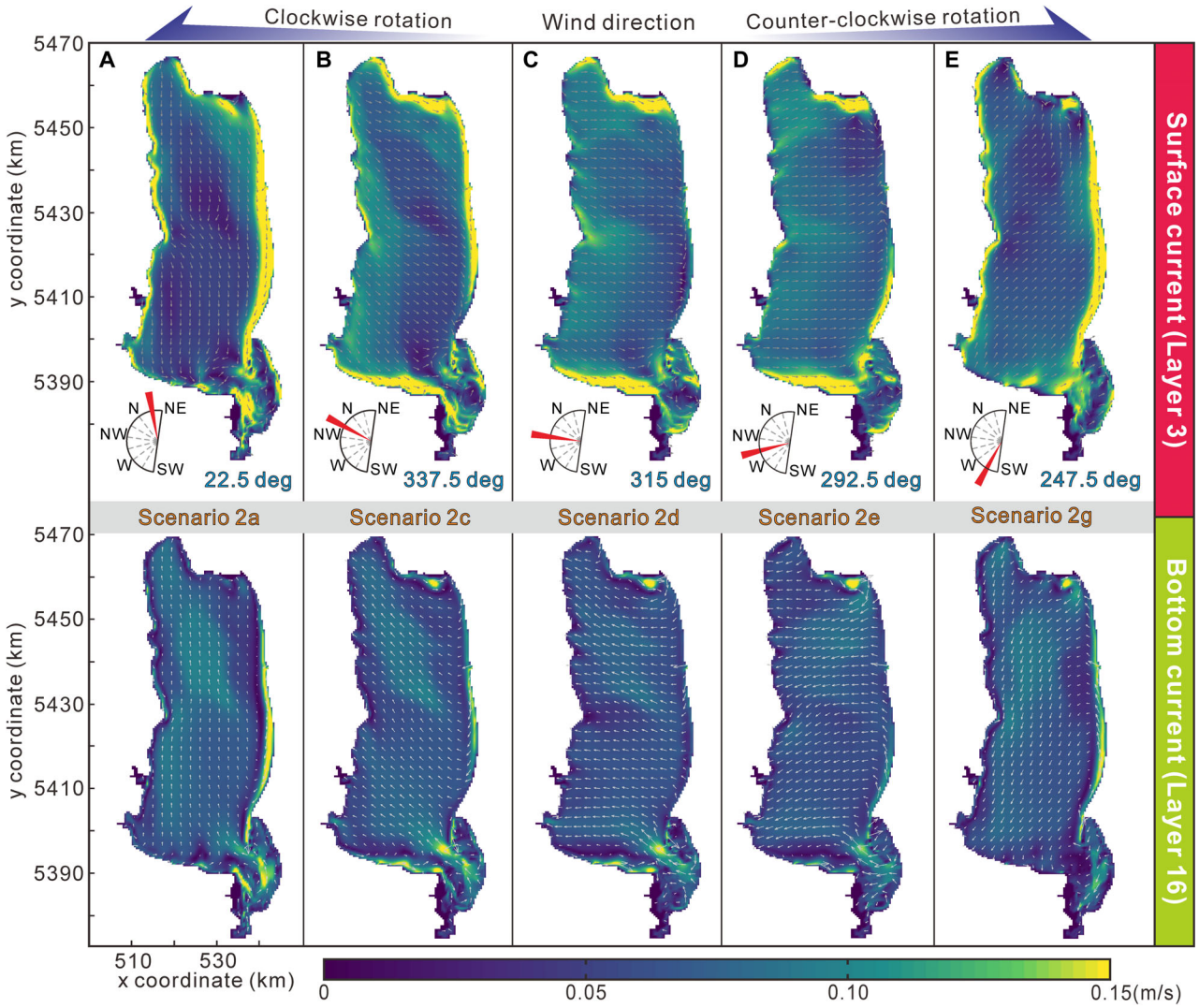

Fig. 5. Flow circulations at steady state, including both magnitude and vector, for five wind direction scenarios (22.5°, 360°, 315°, 270° and 247.5°). The upper part of the figure corresponds to layer 3 while the lower part of the figure corresponds to layer 16.

the flow velocity of both surface and bottom currents varied sharply (Fig. 6D to G). Overall, the circulation pattern remains similar in the cross-sectional views (Fig. 6A to C). However, as the wind speed increases, the difference of surface flow velocity (represented by layer 3) between the downwind and upwind shores becomes more pronounced.

The resulting SSC profiles (Fig. 7) indicate that, as wind velocities rise from 9 m/s to 18 m/s, the proportion of areas with zero SSC gradually decreases, while a discernible boundary separates these areas from those with non-zero SSC. This boundary shifts towards the upwind shore as the wind speed increases.

Variable bathymetry (Scenario 4, a–c)

Simulation results from scenarios with bathymetric variations provide insight into the sensitivity of simulated flow patterns on water depth. The main flow patterns observed in the scenario with two depth centres (S4a) are similar to those of Scenario 2d. More specifically, an additional faster bottom flow developed in the second depth centre (Fig. 8A). In Scenario 4b where the

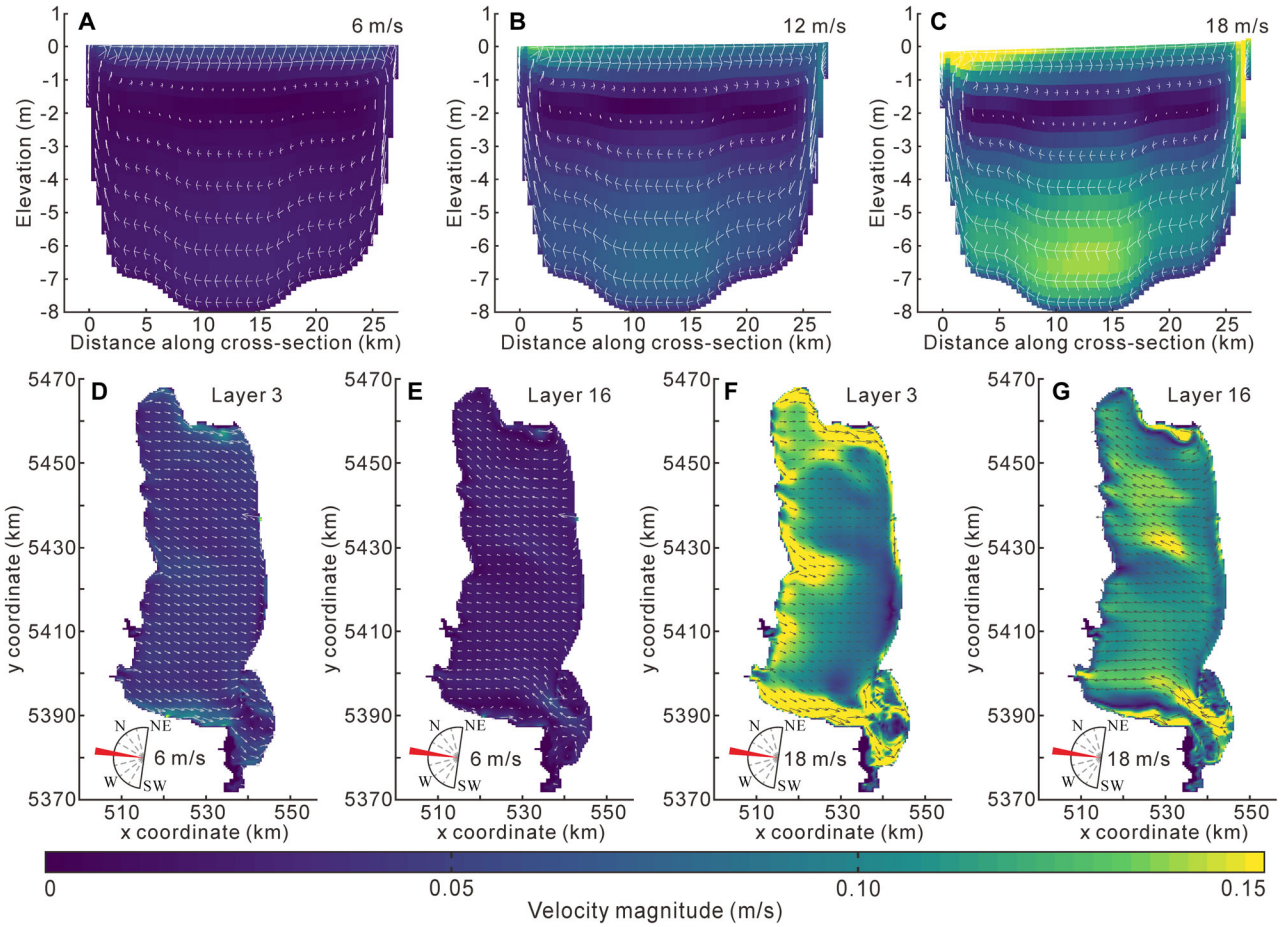

Fig. 6. (A) to (C) Flow circulations in cross-section view (y = 140, see location in Fig. 3A) with different wind velocities of 6 m/s, 12 m/s and 18 m/s in 315° wind direction (Scenarios 3a, 2d and 3d, respectively). (D) to (G) Flow circulation in plane-view of surface current (layer 3) and bottom current (layer 16) for Scenarios 3a and 3d.

depth centre is increased from a maximum depth of 8 to 15 m, the impacts of the depth centre on flow velocities are further amplified (Figs 8B and 9B). Scenario 4c simulates an overall increased water depth throughout the entire lake instead of solely the depth centre as in Scenario 4b (Fig. 8C). In this scenario, surface current velocities are faster than those in the scenario with original bathymetry, but bottom current velocities only show minor changes (Figs 8C and 9C).

Vertical structure of hydrodynamic profiles from Scenario 4 are shown in Fig. 9A to C. Although changes were applied to the bathymetry, the hydrodynamic profile is almost constant with Scenario 2d featured by the original bathymetry (Fig. 6A to C). The bottom current takes up the largest proportion of the depth profile and is overlain by a reduced-flow zone, while the surface current occupies the smallest portion of the water column. However, the thickness of bottom currents increases as the water depth has been deepened (Fig. 9B and 9C). Additionally, the deepened depth centre in Scenario 4b, is characterized by locally faster bottom currents when compared to the shallower depth centre in Scenario 2d (Figs 5C and 9B).

The SSC profile for the depth centre in Scenario 4a (Fig. 9D) is nearly equal to that in Scenario 2d (Fig. 7B) although they have different depth centre locations. As shown in Fig. 9E, however, the SSC boundary does not reach the depth centre and is limited only to the eastern nearshore zone (S4b). Similarly, the SSC remains confined to the shallow water area along the south-east coast in Scenario 4c where the overall depth of the lake basin is increased (Fig. 9F).

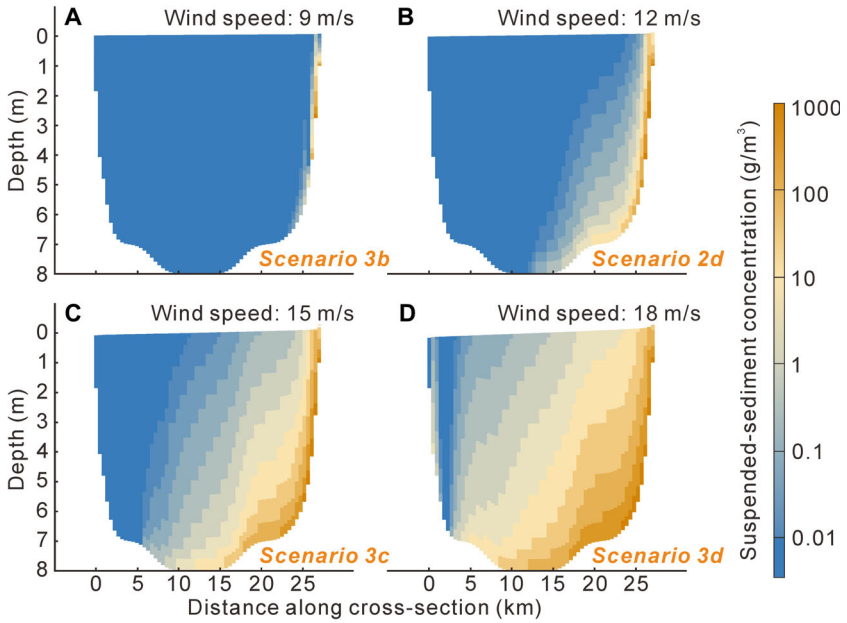

Fig. 7. Cross-sections of suspended sediment concentration (y = 140, see location in Fig. 3A) under different wind velocities. (A) Scenario 3b; (B) Scenario 2d; (C) Scenario 3c; (D) Scenario 3d.

Simplified shoreline shape (Scenario 5, a–c)

To assess the impact of shoreline rugosity on flow conditions in Lake Hulun, a scenario using a simplified rectangular lake outline was implemented (Fig. 10A). A wind speed of 12 m/s was simulated that led to near-shore surface current velocities surpassing 0.25 m/s (Fig. 10B). For a wind direction that is exactly perpendicular to the long-axis shore (270°, S5a), two flow circulations developed at either side of the lake ends (Fig. 10C), together with sediment transport along the short-axis shores (Fig. 10D). Eastward surface currents in the central part of the lake slow down sharply as they approach the downwind shore, encountering a return current originating from the shore (Fig. 10B). Bottom currents maintain a consistent flow direction at the central part of the lake (Fig. 10C). The downwind shore is mainly dominated by onshore-directed sediment transport, but the sediment transport direction gradually diffuses towards both the northern and southern lake ends (Fig. 10D). In addition, the most intensive sediment transport occurs at the north-east and south-east corners where sediments divert back towards the lake centre.

When the wind direction is oblique to the long-axis shore (S5b–S5c), surface currents developed around the shoreline are faster than the central part of the lake, while the fastest bottom current only occurs at the eastern shore (Figs 10B, 10C and S3). At the bottom layer, a fast flow (over 0.15 m/s) develops in the opposite direction of the prevailing wind direction where longshore currents converge (Figs 10C and S3B). Sediment transport is dominated along the downwind shores, especially at the south-eastern corner (Fig. 10D).

Extended hydrodynamic time (Scenario 6, a–b)

Results for long-term sediment erosion and accumulation are represented by Scenarios 6a and 6b with half-year simulation periods. With a shifting wind field in Scenario 6a, occurrence of sediment erosion and accumulation can be observed along the entire shoreline (Fig. 11A). Compared with the nearshore zone where erosion and sedimentation have a tendency to reach a state of equilibrium, net sediment accumulation is observed for the depth centre (Fig. 11C).

In the subsequent simulation (S6b), which set a constant easterly wind direction, sediments mainly accumulate along the western shore (Fig. 11B). Sediments primarily accumulate in the nearshore zone where, respectively, the proximal and distal cumulative sedimentation are about 0.25 m and 0.1 m thick (Fig. 11D). The area between these nearshore depositional bands shows net erosion. In addition, two

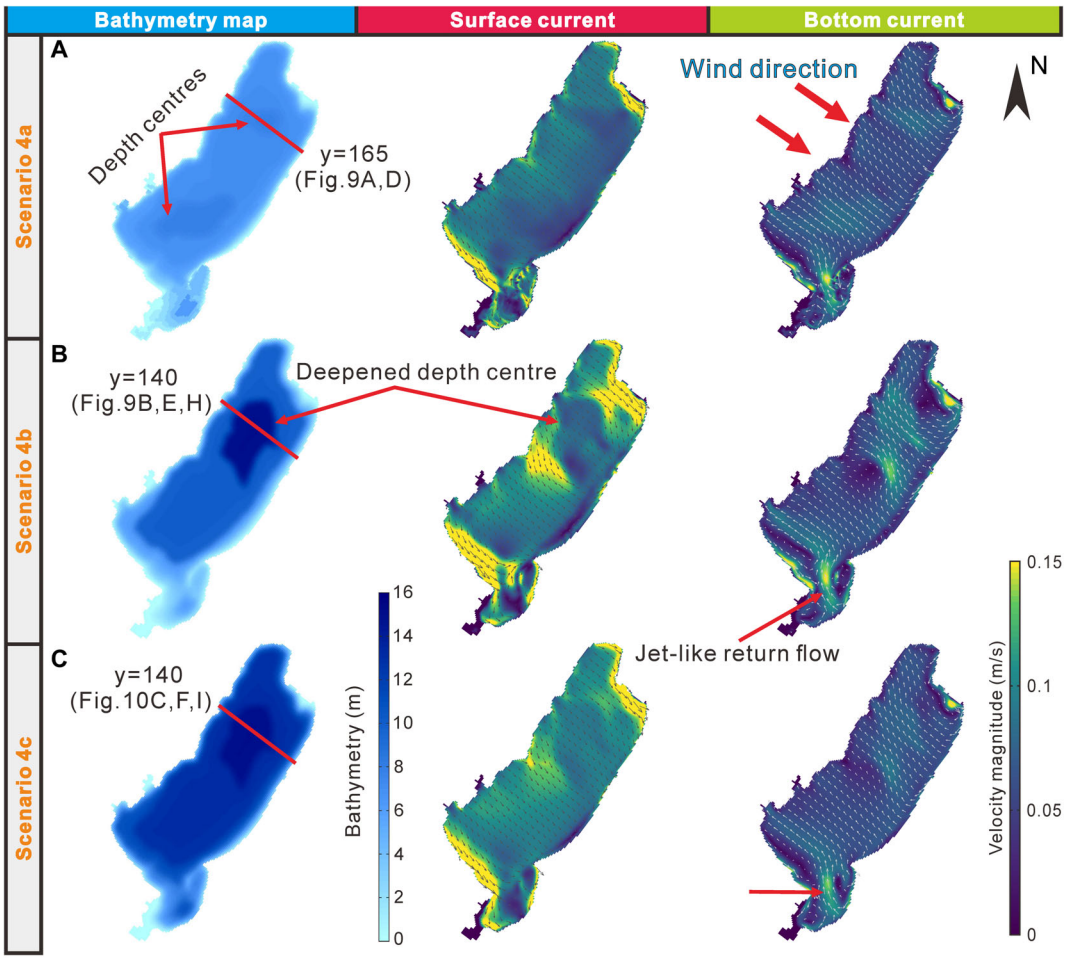

Fig. 8. Bathymetric maps, hydrodynamics of surface currents and bottom currents in (A) Scenario 4a with two depth centres. (B) Scenario 4b with a deepened depth centre. (C) Scenario 4c with an overall increased depth.

elongated sediment accumulations were observed in the offshore zone (Fig. 11D).

INTERPRETATION

Wind-driven hydrodynamics of the Lake Hulun model

The results indicate that flow circulation patterns of Lake Hulun are sensitive to wind directions (Fig. 5), but less sensitive to changes in wind speed (Fig. 6). Observations for Scenario 2 further indicate that flow patterns adjust to new wind directions within 12 h (Fig. 5). All scenarios with wind waves exhibit consistent surface and bottom currents with opposite flow directions at the central part of Lake Hulun. Through wind friction on the lake surface, the winds can generate waves and stable surface flows that are aligned in their directions. The wind-induced waves approaching the shore can generate orbital motion which can create return flows near the bottom layers. This return current can be further enhanced by the water level set-up. The hydrodynamic profiles of Lake Hulun also exhibit a downwelling process that occurs along the downwind slope (Fig. 6A to C). The return flows then move westward along the lake floor, spreading across the entire lake.

The flow velocity of the surface layers along the upwind shore is higher than the downwind shore when the wind is perpendicular to the long-axis shore (Figs 5 and 10B). The authors suggest that this may be caused by currents sourced from return flows in the bottom layers

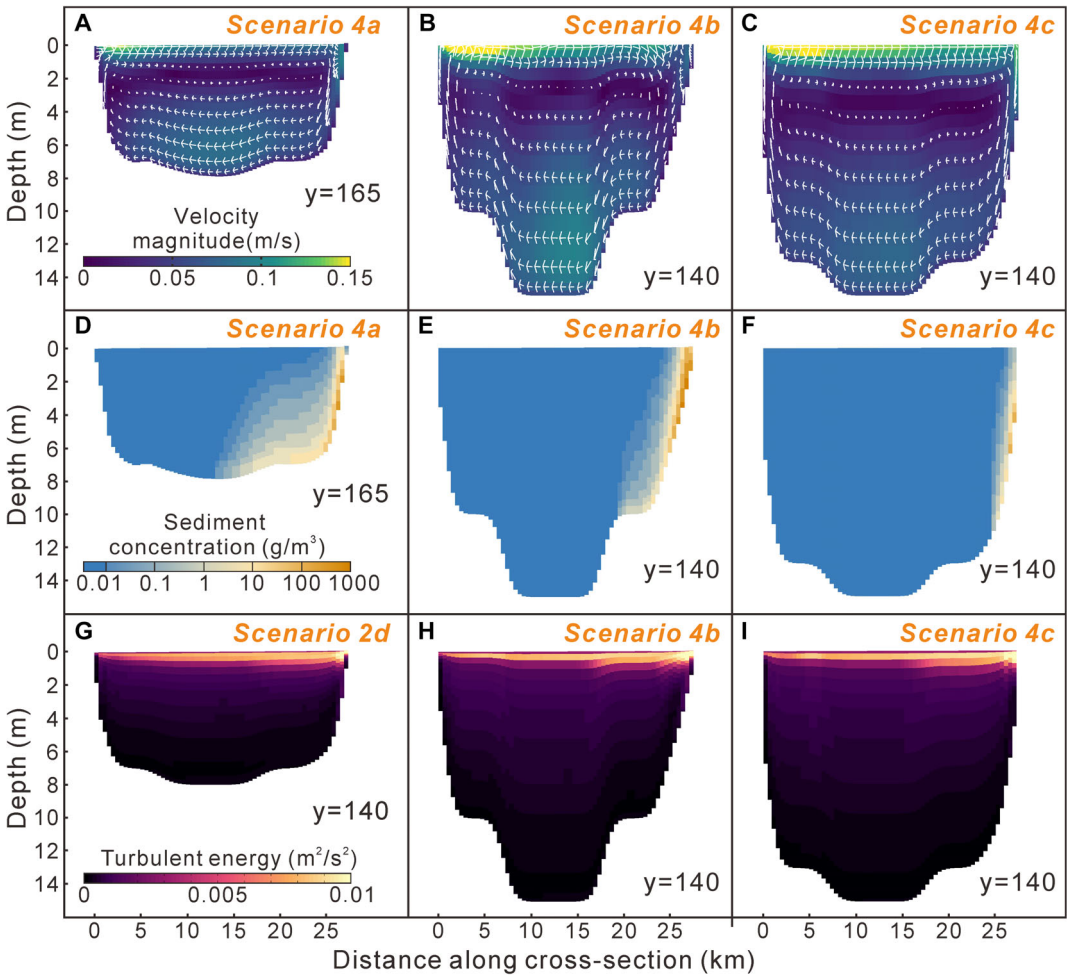

Fig. 9. (A) to (C) Cross-sections of flow circulations in Scenarios 4a to 4c. White arrows are velocity vectors. (D) to (F) Cross-sections of suspended sediment concentration in Scenarios 4a to 4c. (G) to (I) Cross-sections of turbulent energy in Scenario 2d with original bathymetry and Scenarios 4b and 4c with changed bathymetry.

that surge upward towards the surface layer on the upwind side of the lake (Fig. 6A to C), ultimately forming a complete vertical flow circulation. This flow circulation only focuses on the vertical boundaries and lateral slopes, but has little influence in the middle portion of the water column. Such a reduced-flow zone within the flow circulation is probably due to a velocity gradient induced by the friction between the surface and bottom layers with opposite flow directions.

Longshore currents also emerge where wind waves obliquely approach the shore due to the wave-breaking process (Longuet-Higgins, 1970). Unlike the central part of the lake where surface and bottom currents have opposite flow directions, the longshore current is characterized by a consistent flow direction in the vertical profile, represented by layer 3 and layer 16 (Fig. 5). Cross-shore currents are limited within 3 km from the shoreline (Fig. 12A). Where longshore currents converge (for example, in the south corner of Lake Hulun), a strong jet-like return current flowing towards the lake centre develops (Fig. 5A to C). This phenomenon is unlikely to be generated by the unique shoreline shape of Lake Hulun because such a jet-like return current is also exhibited in the scenario with a simplified shoreline shape (Figs 10C and S3B). Such 'jet-like' return current forms when opposing longshore currents meet, creating an intensified offshore-directed

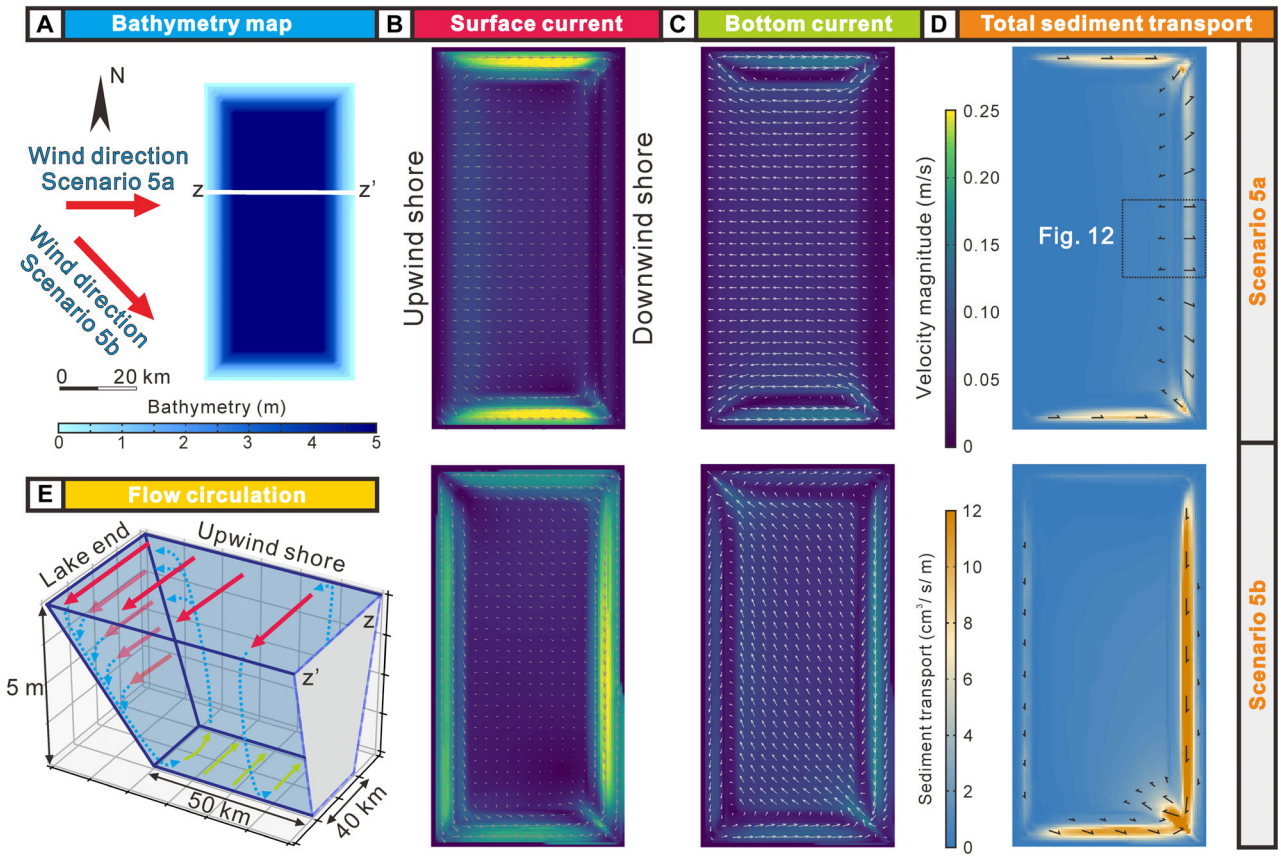

Fig. 10. (A) Bathymetric map for scenarios with an idealized shoreline. (B) Hydrodynamic characteristics of surface currents in Scenarios 5a and 5b. (C) Hydrodynamic characteristics of bottom currents in Scenarios 5a and 5b; (D) Total sediment transport magnitudes ($cm^3/s/m$) and vectors in in Scenarios 5a and 5b. (E) Three-dimensional schematic diagram of flow circulation. Red and green arrows indicate surface and bottom flows, respectively; blue arrows indicate upwelling and downwelling flows.

flow that transports water and sediments back towards deeper water.

Bathymetric-influenced hydrodynamics of the Lake Hulun model

The depth centre in scenarios of Lake Hulun slows down the surface current and speeds up the bottom current. This phenomenon can be interpreted by the Bernoulli principle, where the flow tends to bypass the deeper area with relatively higher water pressure. The effect from the depth centre becomes more obvious in Scenario 4b with a deepened depth centre compared with the original bathymetry (Fig. 8B). As the surface currents slow down above the depth centre, the bottom currents must accelerate to compensate for the conservation of momentum. Therefore, the flow behaviours at the central part of the lake will be influenced by changes in the characteristics of the depth centre (for example, amount, location, depth value) as shown in Fig. 8A and 8B. However, the longshore currents and the jet-like return currents at the nearshore areas are consistent between Scenario 4 with varied bathymetry and other scenarios with original bathymetry.

When the overall water depth is changed from a maximum of 8 m to 15 m (S4c), the circulation pattern at the bottom layers (represented by layer 16) remains approximately consistent. However, flow velocities at the surface layers (represented by layer 3) in Scenario 4c are higher than those in relatively shallower scenarios. It was noticed that surface currents above the reduced-flow zone are always in the upper 1 to 2 m of the water column in every scenario regardless of the difference in

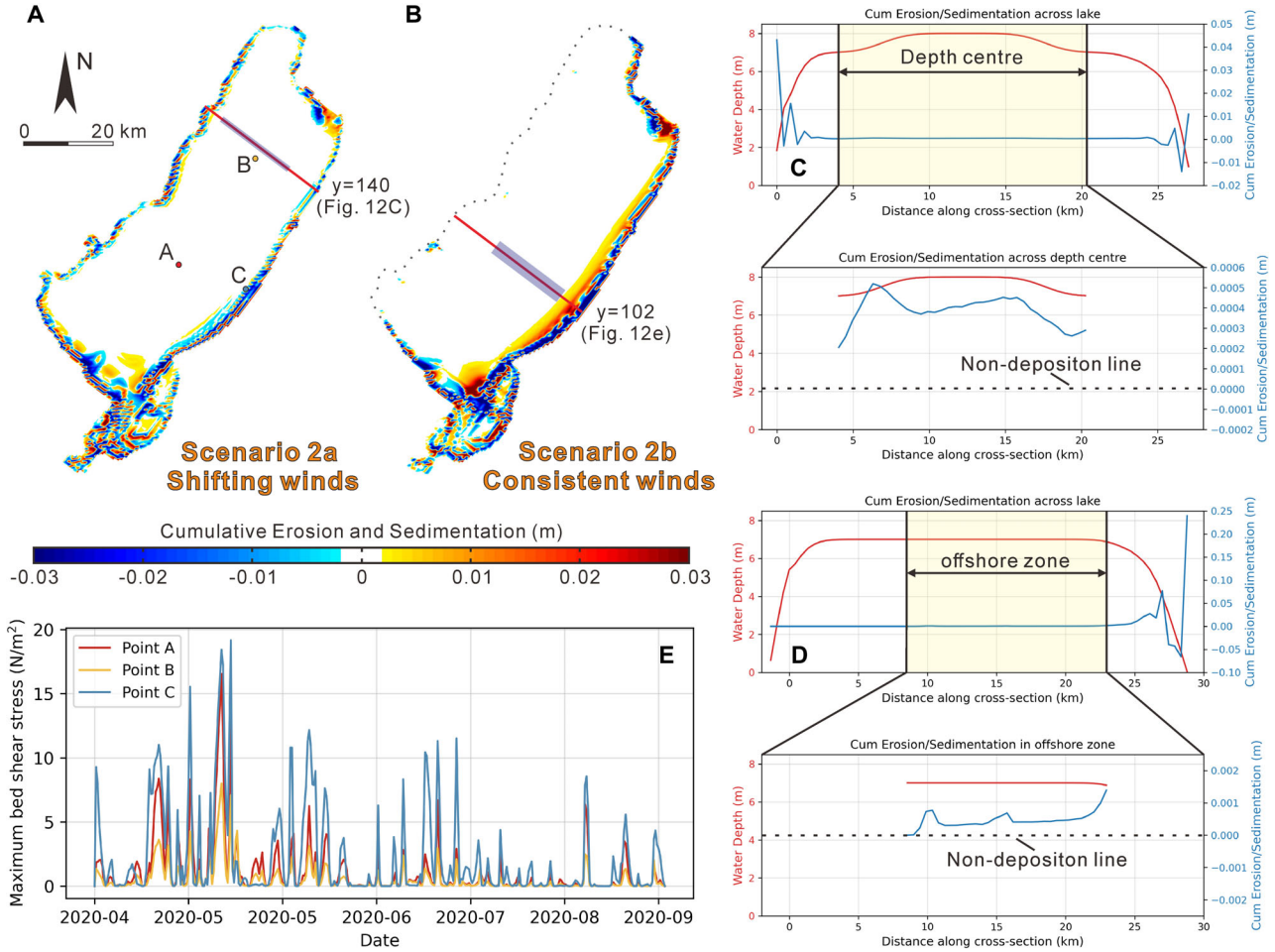

Fig. 11. Plane view of cumulative erosion and sedimentation in: (A) Scenario 6a; and (B) Scenario 6b. Cross-section of cumulative erosion and sedimentation (blue line) and water depth (red line) in: (C) Scenario 6a; and (D) Scenario 6b. (E) Time-series plot of maximum bed shear stress in observation points (see locations in Fig. 11A).

simulated bathymetry (Fig. 9A to C). This is due to the exponential decay of turbulent energy transmitted from the winds to the water-body (Fig. 9G to I). Wüest *et al.* (2000) demonstrated that more than 80% of mechanical energy is dissipated in the upper 1.7 m of the water column before it reaches the strongly stratified hypolimnion. Overall, the acquisition of a high-resolution bathymetry in the deeper water zone may be unnecessary when the hydro-sedimentary dynamics along the coastal area are studied. That being said, the general basin morphology significantly influences lake-wide circulation patterns. For instance, the presence of dual depth centres produces distinct deep-water flow structures compared to the single-centre configuration, while maintaining similar nearshore hydrodynamics (Fig. 9A).

Sedimentary dynamics of the Lake Hulun model

Under the condition of 12 m/s wind speed with the original bathymetric map of the lake, combined steady and oscillatory flow (current plus waves) in the depth centre effectively resuspend bed sediments into the water column, as indicated by the SSC distribution (Figs 4 and 7). The relative wave height (Hs/d, where Hs is the significant wave height and d is the water depth) has a positive correlation with the sediment transport when current velocities varied among 0.1 to 0.6 m/s (Van Rijn, 2007b). Because of this, a smaller Hs/d value will be created either by decreasing wind speed (S3a–S3b) or by increasing water depth (S4b–S4c), resulting in a negligible SSC value (<0.01 g/m^3) in the deep areas (Figs 7A, 9E and 9F).

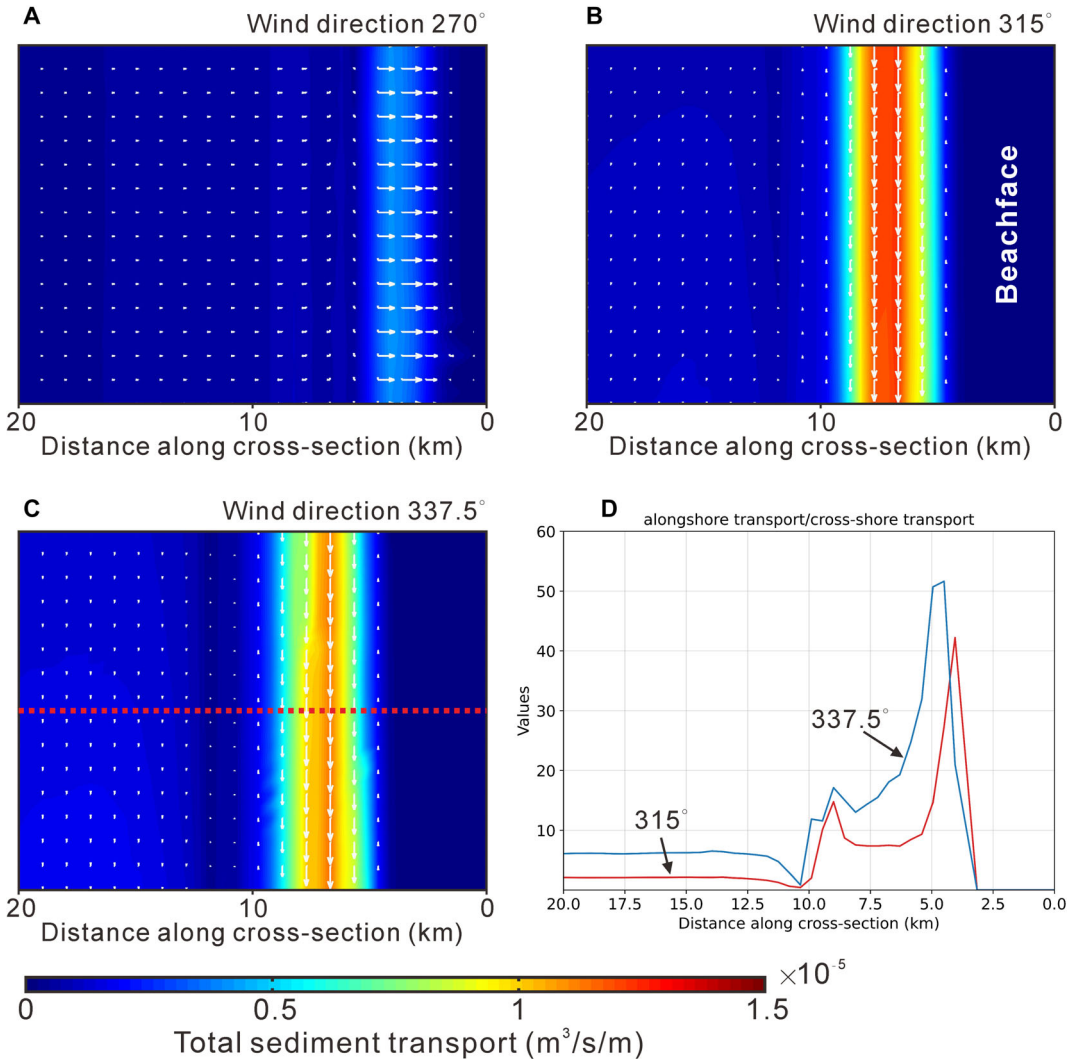

Fig. 12. Zoom-in view of total sediment transport in the nearshore area of the idealized model when the wind direction is: (A) 270°; (B) 315°; and (C) 337.5°. (D) The ratio between longshore transport and cross-shore transport across the nearshore area (see location in Fig. 12C).

Regardless of whether the wind direction is perpendicular or oblique to the shore, most sediments are transported along the downwind shore where the maximum bed shear stress (observation point C) is much higher than that in the deep-water zone (Figs 10D and 11E). This could be due to the wave shoaling and breaking process in the nearshore zone which generates sufficient dissipation energy leading to an increase in bed shear stresses and higher rates of sediment resuspension (Hilton *et al.*, 1986; Van Rijn, 2013). When the wind direction is perpendicular to the downwind shore, sediments are mainly transported in an onshore direction (Fig. 12A). The authors interpret that the onshore-directed sediment transport is due to the swash process induced by the asymmetry of the orbital motion of water at the surf zone where waves completely break (Fig. 13A). The sediment transport behaviour in the nearshore area is similar to that in the oceanic coast where sediments also move in an offshore direction (Fig. 12A) or along the shore, depending on the wind direction (Fig. 12B and 12C).

DISCUSSION

Hydro-sedimentary dynamics in Lake Hulun

Under the idealized wind conditions (wind direction perpendicular to the long axis of the lake), the circulation pattern for a shallow and

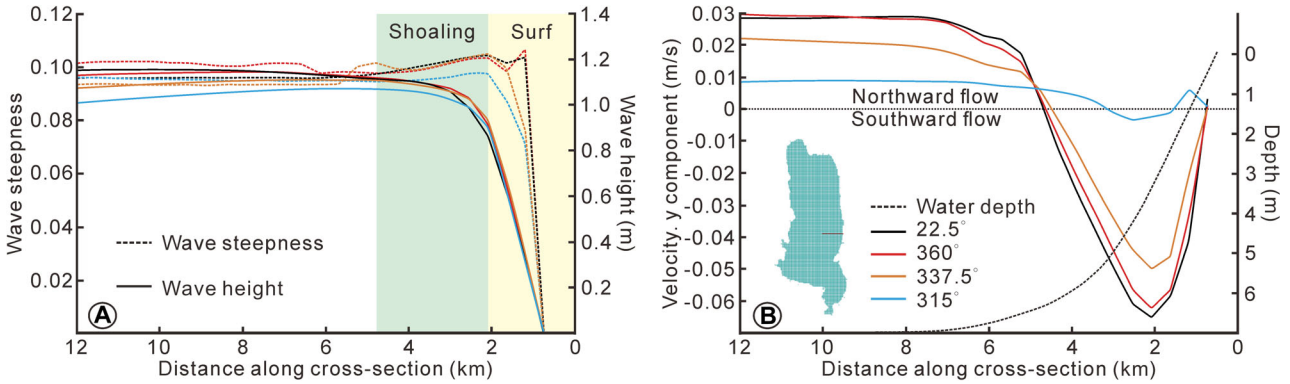

Fig. 13. Profile of: (A) wave conditions; and (B) bottom flow velocity (σ layer 20) in 'y' component under different wind directions (Scenarios 2a to 2d). Dashed line indicates the water depth. The minus value of velocity indicates southward currents.

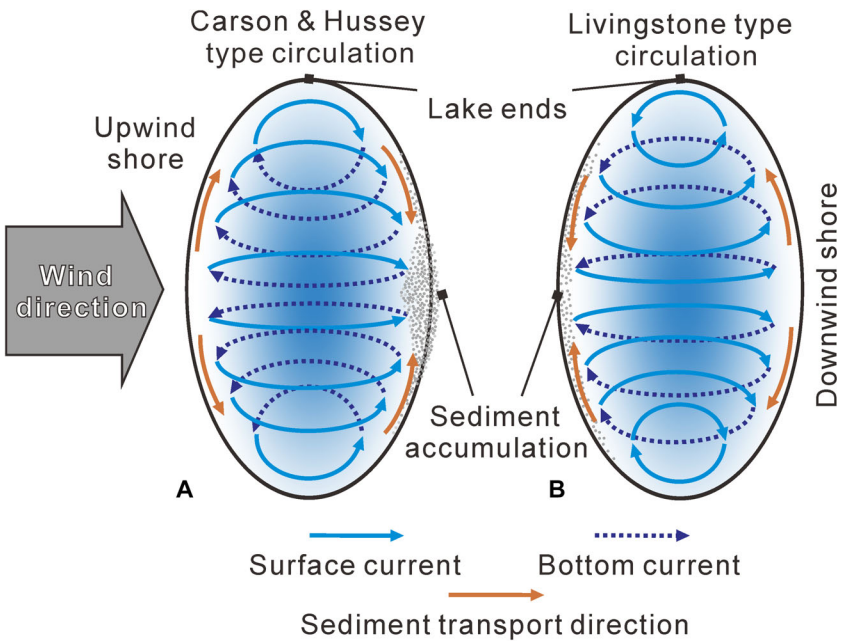

Fig. 14. Two types of flow circulation patterns formed by unidirectional winds in shallow lakes: (A) Carson and Hussey (CH-type) circulation; and (B) Livingstone (L-type) circulation. They lead to opposite flow directions around lake ends and cause different sediment accumulation patterns. The blue shade indicates the deeper area (Redrawn form Ohara *et al.*, 2022).

oval lake was first mentioned by Livingstone (1954) when conceptualizing the effective acceleration of currents around lake ends (short-axis shores) by wind-induced return rip currents (L-type circulation, Fig. 14B). Sediments driven by this L-type circulation tend to accumulate on the upwind shore. In contrast, Carson & Hussey (1962) proposed a reverse circulation pattern (CH-type circulation), in which the surface flow direction around the lake ends aligns with the wind direction. Sediments in CH-type circulation tend to accumulate at the central part of the downwind shore (Fig. 14A), which can explain the existence of peat and sediment bars near the downwind shore (Ohara *et al.*, 2022).

In Scenario 5a with a simplified rectangular lake shape, the observed longshore currents at the lake end undergo downwelling, forming the return bottom current at the deeper zone, (Fig. 10C). The return currents near the bottom then surge upward towards the top layer on the upwind shore and connect to the longshore current, completing a CH-type circulation (Figs 10E and 13A). Sediments from the downwind shore are not expected to be transported towards the central part, as described in the CH-type model

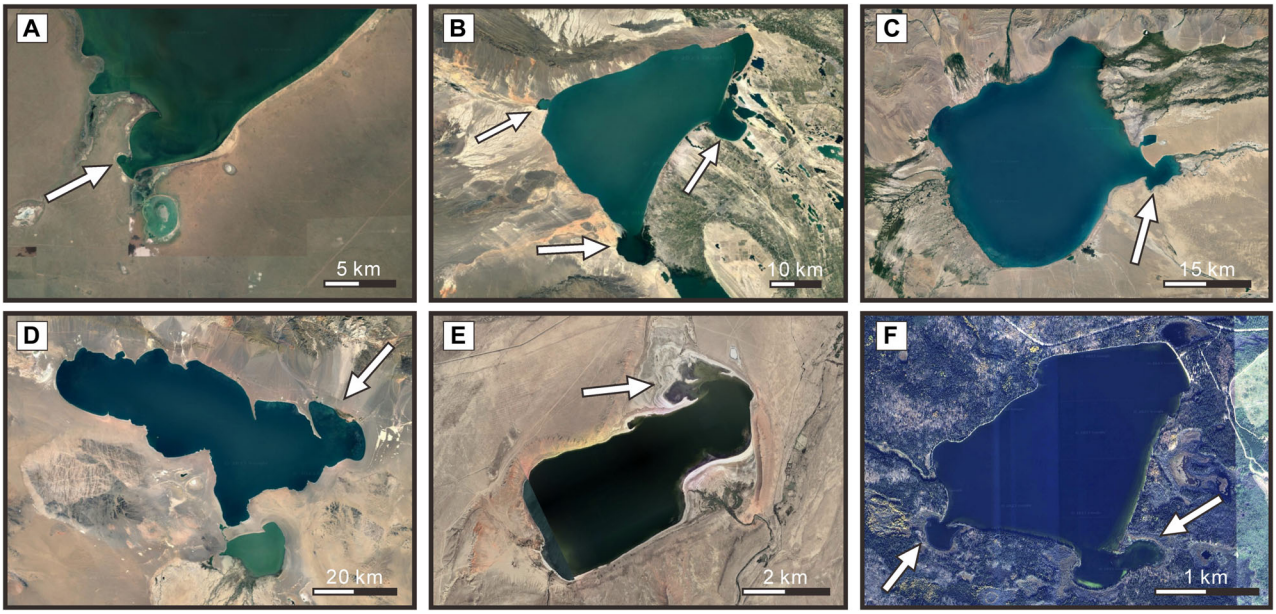

Fig. 15. Natural examples of lakes with semi-enclosed bays surrounded by spits (highlighted with white arrows): (A) Southern corner in Lake Buir, Mongolia; (B) Lake Ulungur, China; (C) Lake Uvs, Mongolia; (D) Lake Khyargas, Mongolia; (E) Lake Kyzylkol, Kazakhstan; (F) Lake Matheson, Canada.

(Carson & Hussey, 1962), but they have simple onshore and offshore transports (Fig. 10D). However, in this study, the shoreline setup is not an oval shape, which may have a significant difference in its impact when comparing to the CH-type circulation model.

It is also worth mentioning that the wind direction will not be completely orthogonal to the lake shore, due to the irregular shoreline and variable wind directions in the real world. As the wind direction becomes oblique to the shoreline, it generates incoming waves with an angle of wave approach, which then produces longshore currents as it flows parallel to the shoreline, becoming the dominant flow type (Fig. 10B and 10C). Longshore drifts on the downwind sides are the dominant mechanism for sediment transport (Fig. 10D). The intensity of longshore drift decreases markedly by 5 cm^3/s/m as the wind direction shifts from 337.5° to 315° (Fig. 12B and 12C). Yet the longshore sediment transport is still about 40 times greater than the cross-shore sediment transport (Fig. 12B).

Other than longshore drifts, bottom sediment drifts in the deeper sections of the lake cannot be neglected for a sedimentation model of WWBs. In a combined flow condition (steady and oscillatory flow), sediment transports are dominantly dependent on the relative wave height rather than simply decided by near-bed flow velocities (Van Rijn, 2007b). For example, in Scenario 6a with a maximum water depth of 8 m, the maximum near-bed flow velocity at observation point B is lower than 0.08 m/s (Fig. 2C), but has a net sediment accumulation at the depth centre (Fig. 11C). In another example, although the near-bed flows reach 0.15 m/s (Fig. 8B), there are no sediments to be resuspended at the depth centre of Lake Hulun with a maximum water depth of 15 m in Scenario 4b (Fig. 9B).

Formation mechanism of the semi-enclosed bay

The semi-enclosed bay in the south-eastern part of Lake Hulun is bordered by two large spits (Fig. 1C). A similar shoreline configuration can be observed in the nearby shallow Lake Buir, located 80 km away from Lake Hulun (Figs 1B and 15A). The cause of such lacustrine landforms has yet to be studied in detail. Because these two lakes have the same orientation and have been influenced by the same prevailing winds, the authors hypothesize that wind-driven flow circulations control the development of such semi-enclosed bays.

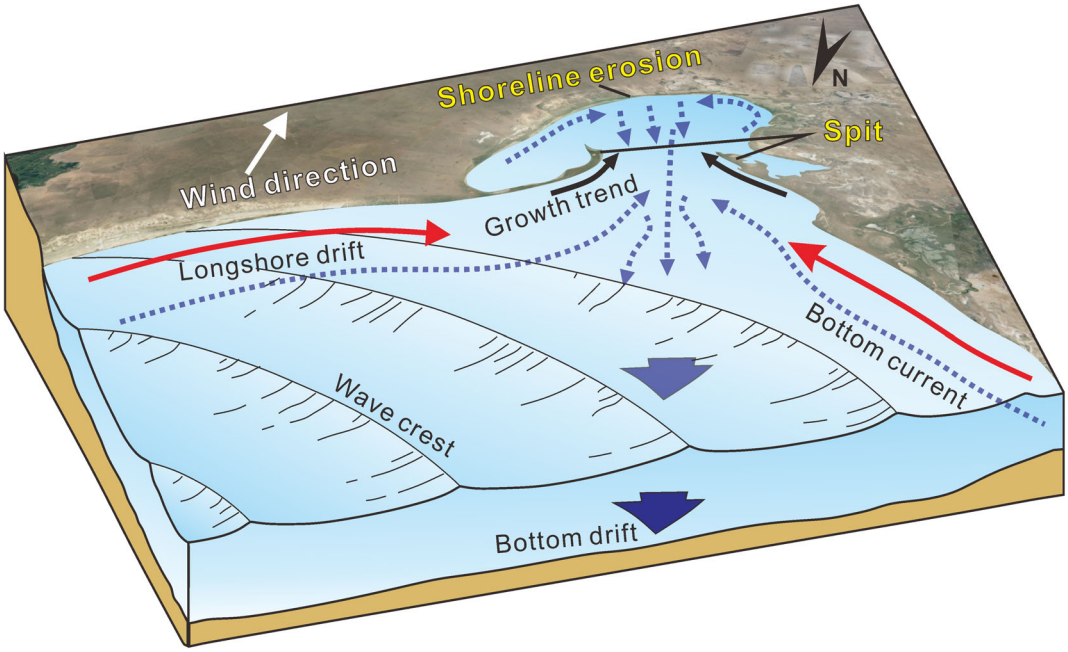

Fig. 16. Conceptual hydro-sedimentation model in the downwind-side corner of Lake Hulun based on simulation results.

Simulation results of the Lake Hulun model show that the longshore currents are strongest when the wind direction is quasi-parallel to the long axis of Lake Hulun (for example, 22.5° or 247.5°, Fig. 5A and 5E). When the wind direction is oblique to the long axis of Lake Hulun (for example, 337.5°), two strong longshore currents simultaneously develop along the spits (Fig. 5B). They interact at the bay mouth and develop a jet-like return current (Fig. 5B). Scenarios with a simplified shoreline shape (S5b–S5c) reveal similar hydrodynamic conditions for the downwind corner (Fig. 11C).

At the convergence point, the combined energy of both longshore currents leads to higher rates of sediment resuspension. Interaction of return currents with local wave action takes the sediment out into the lake centre leading to overall coastal erosion in the southern corner, which effectively over time may become a semi-enclosed bay, although this process could take up to millennia. The authors expect that the semi-enclosed bay in Lake Hulun could become completely closed off with the continuing growth of spits at the bay mouth, indicated by significant sediment transport along both spit growth directions. However, the offshore-directed return current is sufficiently strong to keep the bay mouth open and keep the spits and the bay in a state of equilibrium (Fig. 16). Such hydro-sedimentary dynamics may explain the reason why both Lake Hulun and Lake Buir could develop semi-enclosed bays at their southern corner. The wind-influenced landforms discussed here are also observed in many other cases, including Lake Ulungu in China (Fig. 15B), Lake Uvs and Lake Khyargas in Mongolia (Fig. 15C and 15D), Lake Kyzlkol in Kazakhstan (Fig. 15E), and even Lake Matheson in Canada (Fig. 15F).

Implications and perspectives of lacustrine numerical modelling

Continuous depositional records from the lacustrine basin commonly contain complete palaeogeographical information, such as local climatic changes (Håkanson & Jansson, 1983). This study of Lake Hulun exhibits a net sediment accumulation in the depth centre under a shifting wind field during a non-frozen period (S6a). A similar case from Llyn Conwy (Wales, UK) also shows a patchy distribution of lake sediments within the deeper areas, which is controlled by near-bed currents (Morales-Marin *et al.*, 2018). The simulations herein also show that sediments from the deepest part (8 m depth) of Lake Hulun can be re-suspended by a wind of 12 m/s velocity regardless of the wind direction (Fig. 4), indicating that depositional records will be affected by

wind-driven currents, and therefore is not a continuous record. Only when the depth is 15 m (Scenario 4b) are waves induced by 12 m/s winds unable to resuspend sediments in the depth centre (Fig. 9E).

Under prevailing wind influence, the sediment accumulation pattern is totally different. Two parallel-distributed sediment accumulations were obtained in Scenario 6b, of which the distribution patterns and morphological features are comparable to the bar-trough system in the nearshore area (Wright *et al.*, 1986; Anthony & Aagaard, 2020; Isla *et al.*, 2020). Although they are only several millimetres high, they could become prominent with longer hydrodynamic time or with an increase in wind speed. The presence of a six-month annual frozen period in Lake Hulun introduces temporal discontinuities in sediment transport processes. Computational constraints inherently limit the feasibility of direct morphodynamic simulation across geological timescales (for example, decades, even centuries) without implementing acceleration methods; while morphological acceleration factor method (Morfac) (Lesser *et al.*, 2004) has been widely adopted in contemporary morphodynamic simulations (e.g. Xu *et al.*, 2022; Li *et al.*, 2023; Valencia *et al.*, 2023, 2024). Despite the compelling computational advantages afforded by the Morfac approach, its application should be rigorously and methodically assessed prior to its general acceptance in coastal morphodynamic modelling (Ranasinghe *et al.*, 2011). Considering the complex non-linear coupling between episodic wind forcing and resultant morphological responses, the application of the Morfac method in the present wind-driven shallow lacustrine system may introduce uncertainties. Future investigations would benefit from a more refined model focused on nearshore processes, incorporating appropriate Morfac value to study the long-term development of depositional features for nearshore bars in lacustrine settings.

Numerous studies documented spatial distributions of total organic carbon (TOC), nutrients and pollutes that exhibit differences from the modelled clastic sediment accumulation pattern herein (e.g. Li *et al.*, 2021; Wang *et al.*, 2023; Zhang *et al.*, 2024). This spatial disparity demonstrates that suspended matter distribution within lacustrine systems extends beyond simple wind-driven hydrodynamic controls. Specifically for Lake Hulun, its north-western margin is characterized by elevated vegetation coverage and enhanced topographic gradients, facilitating preferential terrestrial organic carbon flux into this sector of the basin (Li *et al.*, 2021). With little availability of data and monitoring (for example, detailed bathymetry, wind field or water profiles) this study utilized a series of simulations to understand the hydro-sedimentary dynamics of Lake Hulun. When establishing a model setup, the bathymetric maps are always a key problem (Zăinescu *et al.*, 2023). The results from the scenarios with different bathymetry patterns in this study suggest that a high-resolution bathymetric map may not always be needed and that the uncertainty of local depth centres (for example, locations and depth) has limited impact on the overall lake circulation pattern. With access to global geophysical databases, such as *Copernicus* and *HydroLAKES*, the hydro-sedimentary dynamics of other lakes can also be studied through numerical simulation in the future, with only basic bathymetry data. With an increasing wealth of examples and data, it will then be possible to delve deeper into the hydro-sedimentary dynamics of diverse lake types (for example, tectonic and salinity), and to consider various climatic and environmental conditions.

CONCLUSION

This study investigated the hydro-sedimentary dynamics patterns in Lake Hulun, a shallow wind-driven waterbody (WWB), using six groups of simulations of varying scenarios. The main conclusions are as follows:

1 By conducting a comprehensive analysis of the hydrodynamic characteristics of Lake Hulun under varying wind directions (ranging from oblique to perpendicular to the long-axis shoreline), this study reveals that wind inputs have great impacts on the hydrodynamics and sediment dispersal pathways in WWBs. The hydrodynamics in WWBs are mainly influenced by the shift of wind direction, while variation in wind speed determines the flow velocity and suspended sediment concentrations (SSC). Simulated flow patterns and associated sediment transport closely match coastal features observed from satellite images of Lake Hulun.

2 By conducting a comparative analysis of the hydrodynamic characteristics associated with four different bathymetric maps of Lake Hulun, this study reveals that variations in the depth

centres of the lake have low impact on the overall circulation pattern. Particularly, the hydrodynamic features of the shallow water areas, such as the coastal zones, remain largely unaffected. High-resolution bathymetric mapping in deeper water zones is not essential for the study of hydro-sedimentary dynamics along coastal areas.

3 When the wind direction aligns perpendicular to the long-axis shoreline, longshore currents developed at the short-axis shores, together with return currents, form a distinctive CH-type circulation pattern at both lake ends. The sediment transport pattern is in a simple bi-directional (onshore and offshore) movement at the downwind shore. Once the prevailing wind direction is oblique to the long-axis of the lake, longshore currents become the dominant flow type along the downwind shores. The convergence of two longshore currents generates a jet-like return flow from the downwind corner, related to the formation and the equilibrium state of a semi-enclosed bay.

4 Sediments tend to accumulate in the depth centre where increasing water depth reduces wave influence, although enhanced bottom currents may transport and rework these deposits. Parallel-distributed bars develop in the nearshore zone, although their long-term development requires investigation through geological timescale modelling. Long-term simulation faces inherent constraints from seasonal frozen periods of Lake Hulun and computational limitations, while applying the Morfac method requires careful consideration. Recognizing that acquiring comprehensive datasets faces substantial resource requirements and logistical constraints in global-scale lake investigations, this study demonstrates the efficacy of integrating open-access databases with systematic numerical approaches for investigating hydro-sedimentary dynamics across diverse global lake systems despite data-sparse conditions.

ACKNOWLEDGEMENTS

This study was financially supported by National Natural Science Foundation of China (Nos. 41772090 and W2433100). X.X. was supported by China Scholarship Council (No. 202106400055). F.Z. was supported by Center national d'études spatiales (CNES) through the funding of his postdoctoral fellowship. We thank Deltares and Mr Edward Melger for providing access to the Delft3D software, and Dr Ayunda Aulia Valencia for technical support. An earlier version of this manuscript was significantly improved with the help of the Ph.D. dissertation committee members of X.X and Dr Shan Liu. The authors especially acknowledge Chief Editor Dr Piret Plink-Björklund for editorial work. We thank Dr Zhenhua Xu and three anonymous reviewers for their constructive comments and suggestions.

DATA AVAILABILITY STATEMENT

The Delft3D input files used in this study are publicly available in https://doi.org/10.5281/zenodo.14607150.

REFERENCES

Anthony, E.J. and **Aagaard, T.** (2020) The lower shoreface: Morphodynamics and sediment connectivity with the upper shoreface and beach. *Earth Sci. Rev.*, **210**, 103334.

Ao, W., **Dou, H.**, **Yu, C.**, **Wang, W.**, **Wang, Z.**, **Wang, Q.**, **Lu, L.**, **Zhou, X.**, **Han, R.** and **Zou, C.** (2020) The ice cover shapes the spatial and temporal characteristics of water quality in Hulun Lake during winter. *Water Supply*, **20**, 2589–2602.

Arcement, G.J. and **Schneider, V.R.** (1989) *Guide for Selecting Manning's Roughness Coefficients for Natural Channels and Flood Plains*. US Government Printing Office, Washington, DC.

Bengtsson, L. and **Hellström, T.** (1992) Wild-induced resuspension in a small shallow lake. *Hydrobiologia*, **241**, 163–172.

Booij, N., **Ris, R.C.** and **Holthuijsen, L.H.** (1999) A third-generation wave model for coastal regions: 1. model description and validation. *J. Geophys. Res. Oceans*, **104** (C4), 7649–7666.

Cai, Z., **Jin, T.**, **Li, C.**, **Ofterdinger, U.**, **Zhang, S.**, **Ding, A.** and **Li, J.** (2016) Is China's fifth-largest inland lake to dry-up? incorporated hydrological and satellite-based methods for forecasting Hulun lake water levels. *Adv. Water Resour.*, **94**, 185–199.

Carson, C.E. and **Hussey, K.M.** (1962) The oriented lakes of arctic Alaska. *J. Geol.*, **70**, 417–439.

Ceramicola, S., **Rebesco, M.**, **De Batist, M.** and **Khlystov, O.** (2001) Seismic evidence of smallscale lacustrine drifts in Lake Baikal (Russia). *Mar. Geophys. Res.*, **22**, 445–464.

Chen, J., **Wang, J.**, **Wang, Q.**, **Lv, J.**, **Liu, X.**, **Chen, J.** and **Li, N.** (2021) Common fate of sister lakes in Hulunbuir grassland: Long-term harmful algal bloom crisis from multi-source remote sensing insights. *J. Hydrol.*, **594**, 125970.

Cohen, A.S. (2003) *Paleolimnology: The History and Evolution of Lake Systems*, p. 528. Oxford University Press, Oxford.

Deltares. (2021) DELFT3D-FLOW Simulation of multi-dimensional hydrodynamic flows and transport phenomena, including sediments [Online]. Available from:

https://content.oss.deltares.nl/delft3d4/Delft3D-FLOW_User_Manual.pdf.

Fan, C., **Song, C.**, **Liu, K.**, **Ke, L.**, **Xue, B.**, **Chen, T.**, **Fu, C.** and **Cheng, J.** (2021) Century-scale reconstruction of water storage changes of the largest lake in the inner Mongolia plateau using a machine learning approach. *Water Resour. Res.*, **57**, e2020WR028831.

French, C.E., **French, J.R.**, **Clifford, N.J.** and **Watson, C.J.** (2000) Sedimentation-erosion dynamics of abandoned reclamations: the role of waves and tides. *Cont. Shelf Res.*, **20**, 1711–1733.

Gao, H., **Ryan, M.C.**, **Li, C.** and **Sun, B.** (2017) Understanding the role of groundwater in a remote transboundary lake (Hulun lake, China). *Watermark*, **9**, 363.

Gracia, F.J., **Morales, J.A.**, **Castañeda, C.** and **Plomaritis, T.A.** (2021) Shallow lacustrine versus open ocean coastal clastic deposits: Morphosedimentary diagnostic indicators and interpretation. *Sediment. Geol.*, **423**, 105981.

Gracia, F.J., **Castañeda, C.**, **Simarro, G.**, **Calvete, D.** and **Latorre, B.** (2024) Water level control on coastal landform distribution and associated processes in a highly fluctuating shallow lake (Gallocanta Lake, NE Spain). *Earth Surf. Process. Landf.*, **49**, 770–786.

Håkanson, L. and **Jansson, M.** (1983) *Principles of Lake Sedimentology*, p. 316. Springer, Berlin.

Hasselmann, K., **Barnett, T.P.**, **Bouws, E.**, **Carlson, H.**, **Cartwright, D.E.**, **Enke, K.** and **Walden, H.** (1973) Measurements of wind-wave growth and swell decay during the Joint North Sea Wave Project (JONSWAP). Ergaenzungsheft zur Deutschen Hydrographischen Zeitschrift, Reihe A.

Hilton, J., **Lishman, J.** and **Allen, P.** (1986) The dominant processes of sediment distribution and focusing in a small, eutrophic, monomictic lake. *Limnol. Oceanogr.*, **31**, 125–133.

Isla, M.F., **Coronel, M.D.**, **Schwarz, E.** and **Veiga, G.D.** (2020) Depositional architecture of a wave-dominated clastic shoreline (Pilmatué Member, Argentina): Linking dynamics and stratigraphic record of bar-trough systems. *Mar. Pet. Geol.*, **118**, 104417.

Jiang, Z., **Liu, H.**, **Zhang, S.**, **Su, X.** and **Jiang, Z.** (2011) Sedimentary characteristics of large-scale lacustrine beach-bars and their formation in the Eocene Boxing Sag of Bohai Bay Basin, East China. *Sedimentology*, **58**, 1087–1112.

Jiang, Z., **Wang, J.**, **Fulthorpe, C.S.**, **Liu, L.**, **Zhang, Y.** and **Liu, H.** (2018) A quantitative model of paleowind reconstruction using subsurface lacustrine longshore bar deposits–an attempt. *Sediment. Geol.*, **371**, 1–15.

Jin, K.R. and **Ji, Z.G.** (2004) Case study: modeling of sediment transport and wind-wave impact in Lake Okeechobee. *J. Hydraul. Eng.*, **130**, 1055–1067.

Kazancı, N., **Leroy, S.A.G.**, **Öncel, S.**, **İleri, Ö.**, **Toprak, Ö.**, **Costa, P.**, **Sayılı, S.**, **Turgut, C.**, **Kibar, M.** and **Kibar, M.** (2010) Wind control on the accumulation of heavy metals in sediment of Lake Ulubat, Anatolia, Turkey. *J. Paleo.*, **43**, 89–110.

Khazaei, B., **Bravo, H.R.**, **Anderson, E.J.** and **Klump, J.V.** (2021) Development of a physically based sediment transport model for Green Bay, Lake Michigan. *J. Geophys. Res. Oceans.*, **126**, e2021JC017518.

Lesser, G.R., **Roelvink, J.V.**, **van Kester, J.T.M.** and **Stelling, G.S.** (2004) Development and validation of a three-dimensional morphological model. *Coast. Eng.*, **51**, 883–915.

Li, C., **Sun, B.**, **Jia, K.**, **Zhang, S.**, **Li, W.**, **Shi, X.**, **Cordovil, C.M.d.S.** and **Pereira, L.S.** (2013) Multi-band remote sensing based retrieval model and 3D analysis of water depth in Hulun Lake, China. *Math. Comput. Model.*, **58**, 771–781.

Li, Y., **Li, X.**, **Huang, G.**, **Wang, S.** and **Li, D.** (2021) Sedimentary organic carbon and nutrient distributions in an endorheic lake in semiarid area of the Mongolian Plateau. *J. Environ. Manage.*, **296**, 113184.

Li, W., **Colombera, L.**, **Yue, D.** and **Mountney, N.P.** (2023) Controls on the morphology of braided rivers and braid bars: An empirical characterization of numerical models. *Sedimentology*, **70**, 259–279.

Livingstone, D.A. (1954) On the orientation of lake basins [Alaska]. *Am. J. Sci.*, **252**, 547–554.

Longuet-Higgins, M.S. (1970) Longshore currents generated by obliquely incident sea waves: 1. *J. Geophys. Res.*, **75**, 6778–6789.

Luettich, R.A., Jr., **Harleman, D.R.** and **SomlyÓdy, L.** (1990) Dynamic behavior of suspended sediment concentrations in a shallow lake perturbed by episodic wind events. *Limnol. Oceanogr.*, **35**, 1050–1067.

Mao, M. and **Xia, M.** (2020) Particle dynamics in the nearshore of lake Michigan revealed by an observation-modeling system. *J. Geophys. Res. Oceans.*, **125**, e2019JC015765.

Morales-Marín, L.A., **French, J.R.** and **Burningham, H.** (2017) Implementation of a 3D ocean model to understand upland lake wind-driven circulation. *Environment. Fluid Mech.*, **17**, 1255–1278.

Morales-Marin, L., **French, J.**, **Burningham, H.** and **Battarbee, R.** (2018) Three-dimensional hydrodynamic and sediment transport modeling to test the sediment focusing hypothesis in upland lakes. *Limnol. Oceanogr.*, **63**, S156–S176.

Nutz, A., **Schuster, M.**, **Ghienne, J.F.**, **Roquin, C.**, **Hay, M.B.**, **Rétif, F.**, **Certain, R.**, **Robin, N.**, **Raynal, O.**, **Cousineau, P.A.**, **SIROCCO Team** and **Bouchette, F.** (2015) Wind-driven bottom currents and related sedimentary bodies in Lake Saint-Jean (Québec, Canada). *GSA Bull.*, **127**, 1194–1208.

Nutz, A., **Schuster, M.**, **Ghienne, J.F.**, **Roquin, C.** and **Bouchette, F.** (2018) Wind-driven waterbodies: a new category of lake within an alternative sedimentologically-based lake classification. *J. Paleo.*, **59**, 189–199.

Nutz, A., **Schuster, M.**, **Barboni, D.**, **Gassier, G.**, **Van Bocxlaer, B.**, **Robin, C.**, **Ragon, T.**, **Ghienne, J.F.** and **Rubino, J.L.** (2020) Plio-Pleistocene sedimentation in West Turkana (Turkana Depression, Kenya, East African rift system): paleolake fluctuations, paleolandscapes and controlling factors. *Earth Sci. Rev.*, **211**, 103415.

Ohara, N., **Jones, B.M.**, **Parsekian, A.D.**, **Hinkel, K.M.**, **Yamatani, K.**, **Kanevskiy, M.**, **Rangel, R.C.**, **Breen, A.L.** and **Bergstedt, H.** (2022) A new Stefan equation to characterize the evolution of thermokarst lake and talik geometry. *Cryosphere*, **16**, 1247–1264.

Ranasinghe, R., **Swinkels, C.**, **Luijendijk, A.**, **Roelvink, D.**, **Bosboom, J.**, **Stive, M.** and **Walstra, D.** (2011) Morphodynamic upscaling with the MORFAC approach: Dependencies and sensitivities. *Coastal Eng.*, **58**, 806–811.

Schuster, M. and **Nutz, A.** (2018) Lacustrine wave-dominated clastic shorelines: modern to ancient littoral landforms and deposits from the Lake Turkana Basin (East African Rift system, Kenya). *J. Paleo.*, **59**, 221–243.

Schuster, M., **Roquin, C.**, **Moussa, A.**, **Ghienne, J.F.**, **Duringer, P.**, **Allenbach, B.** and **Bouchette, F.** (2014)

Shorelines of the Holocene Megalake Chad (Africa, Sahara) investigated with very high resolution satellite imagery (Pléiades): example of the Goz Kerki Paleo-Spit. *Revue française de photogrammétrie et de télédétection*, **208**, 63–68.

Storms, J.E.A., **Beylich, A.A.**, **Hansen, L.** and **Waldmann, N.** (2020) Source to sink reconstruction of a Holocene fjord-infill: Depositional patterns, suspended sediment yields, wind-induced circulation patterns and trapping efficiency for Lake Strynevatnet, Inner Nordfjord, Norway. *Deposition. Rec.*, **6**, 471–485.

Sun, H., **Zang, S.**, **Sun, D.**, **Zhang, K.** and **Sun, L.** (2018) Grain-size characteristics and their environmental significance of Hulun Lake sediments. *Sci. Geograph. Sin.*, **38**, 1570–1578 (In Chinese).

Valencia, A.A., **Storms, J.E.A.**, **Walstra, D.-J.**, **van der Vegt, H.** and **Jagers, H.R.A.** (2023) The impact of clastic synsedimentary compaction on fluvial-dominated delta morphodynamics. *Deposition. Rec.*, **9**, 233–252.

Valencia, A.A., **Storms, J.E.A.**, **Jagers, H.R.A.** and **van der Vegt, H.** (2024) The influence of syn-depositional compaction on clastic sediment distribution in river-dominated deltas: A modelling study. *Deposition. Record.*, **20**, 1–18.

Van Rijn, L.C. (2007a) Unified view of sediment transport by currents and waves. I: Initiation of motion, bed roughness, and bed-load transport. *J. Hydraul. Eng.*, **133**, 649–667.

Van Rijn, L.C. (2007b) Unified view of sediment transport by currents and waves. II: Suspended transport. *J. Hydraul. Eng.*, **133**, 668–689.

Van Rijn, L.C. (2013) Simple general formulae for sand transport in rivers, estuaries and coastal waters, 1–16. Retrieved from www.leovanrijn-sediment.com.

Wagner, B., **Aufgebauer, A.**, **Vogel, H.**, **Zanchetta, G.**, **Sulpizio, R.** and **Damaschke, M.** (2012) Late Pleistocene and Holocene contourite drift in Lake Prespa (Albania/F.Y.R. of Macedonia/Greece). *Quat. Int.*, **274**, 112–121.

Wang, J., **Jiang, Z.**, **Xian, B.**, **Chen, J.**, **Wang, X.**, **Xu, W.** and **Liu, H.** (2018) A method to define the palaeowind strength from lacustrine parameters. *Sedimentology*, **65**, 461–491.

Wang, X., **Fang, C.**, **Song, K.**, **Lyu, L.**, **Li, Y.**, **Lai, F.**, **Lyu, Y.** and **Wei, X.** (2023) Monitoring phycocyanin concentrations in high-latitude inland lakes using Sentinel-3 OLCI data: The case of Lake Hulun, China. *Ecol. Indic.*, **155**, 110960.

Wang, L., **Schuster, M.**, **Xin, S.**, **Zainescu, F.**, **Xue, X.**, **Storms, J.E.A.**, **May, J.H.**, **Nutz, A.**, **van der Vegt, H.**, **Bozetti, G.** and **Jiang, Z.** (2024) Littoral landforms of Lake Hulun and Lake Buir (China and Mongolia): Wind-driven hydro-sedimentary dynamics and resulting clastics distribution. *J. Palaeogeogr.*, **13**, 309–326.

Wright, L., **Nielsen, P.**, **Shi, N.** and **List, J.** (1986) Morphodynamics of a bar-trough surf zone. *Mar. Geol.*, **70**, 251–285.

Wüest, A., **Piepke, G.** and **Van Senden, D.C.** (2000) Turbulent kinetic energy balance as a tool for estimating vertical diffusivity in wind-forced stratified waters. *Limnol. Oceanogr.*, **45**, 1388–1400.

Xiao, J., **Chang, Z.**, **Wen, R.**, **Zhai, D.**, **Itoh, S.** and **Lomtatidze, Z.** (2009) Holocene weak monsoon intervals indicated by low lake levels at Hulun lake in the monsoonal margin region of northeastern Inner Mongolia, China. *Holocene*, **19**, 899–908.

Xu, Z., **Plink-Björklund, P.**, **Wu, S.**, **Liu, Z.**, **Feng, W.**, **Zhang, K.**, **Yang, Z.** and **Zhong, Y.** (2022) Sinuous bar fingers of digitate shallow-water deltas: Insights into their formative processes and deposits from integrating morphological and sedimentological studies with mathematical modelling. *Sedimentology*, **69**, 724–749.

Xue, X., **Zhang, Y.**, **Jiang, Z.**, **Wang, L.**, **Wang, S.** and **Jiang, H.** (2021) Wave and storm signals in a lacustrine succession and their relationship to paleowind direction (Tanan depression, Mongolia, Early Cretaceous). *Sediment. Geol.*, **419**, 105911.

Zăinescu, F., **Van der Vegt, H.**, **Storms, J.**, **Nutz, A.**, **Bozetti, G.**, **May, J.H.**, **Cohen, S.**, **Bouchette, F.**, **May, S.M.** and **Schuster, M.** (2023) The role of wind-wave related processes in redistributing river-derived terrigenous sediments in Lake Turkana: A modelling study. *J. Great Lakes Res.*, **49**, 368–386.

Zhang, H., **Li, Y.**, **Yao, B.**, **Huang, Y.**, **Wang, S.** and **Ni, S.** (2024) Untangling the coupling effect of water quality and quantity on lake algal blooms in Lake Hulun from a dual perspective of remote sensing and sediment cores. *J. Hydrol.*, **645**, 132141.

Zheng, J., **Ke, C.**, **Shao, Z.** and **Li, F.** (2016) Monitoring changes in the water volume of Hulun Lake by integrating satellite altimetry data and Landsat images between 1992 and 2010. *J. Appl. Remote Sens.*, **10**, 16029.

Manuscript received 16 April 2024; revision accepted 7 January 2025

Supporting Information

Additional information may be found in the online version of this article:

Figure S1. (A, B) Wave-dominated landforms at north-western coast. (C) Barrier island at the river mouth area of Xinkai River. (D) Artificial dam at the upstream part of Xinkai River. (E) Beach deposits at the south-east coast and the aeolian deposits behind the beach.

Figure S2. Flow circulations at both the surface layer and bottom layer in (A, B) scenario 3b and (C, D) scenario 3f.

Figure S3. Flow circulations at both the (A) surface layer and (B) bottom layer in scenario 5c.